A model for microbial phosphorus cycling in bioturbated marine sediments: significance for phosphorus burial in the early Paleozoic

Andrew W. Dale [a], Richard A. Boyle [b], Timothy M. Lenton [c], Ellery D. Ingall [d], Klaus Wallmann [a]

[a] GEOMAR Helmholtz Centre for Ocean Research Kiel, Wischhofstrasse 1–3, 24148 Kiel, Germany

[b] Institute of Biology and Nordic Centre for Earth Evolution, University of Southern Denmark, Campusvej 55, 5230 Odense M, Odense, Denmark

[c] Earth System Science group, College of Life and Environmental Sciences, University of Exeter, Laver Building (Level 7), North Park Road, Exeter EX4 4QE, UK

[d] School of Earth and Atmospheric Sciences, Georgia Institute of Technology, Atlanta, Georgia 30332-0340, USA

Corresponding author: A. W. Dale (adale@geomar.de)

Key points

- An empirical diagenetic model includes redox-dependent P storage by microorganisms
- Sediment mixing and burrowing by animals strongly enhances P burial
- Supporting evidence for a decrease in oceanic P inventory in the early Paleozoic

Abstract

A diagenetic model is used to simulate the diagenesis and burial of particulate organic carbon (C_{org}) and phosphorus (P) in marine sediments underlying anoxic versus oxic bottom waters. The latter are physically mixed by animals moving through the surface sediment (bioturbation) and ventilated by burrowing, tube-dwelling organisms (bioirrigation). The model is constrained using an empirical database including burial ratios of C_{org} with respect to organic P (C_{org}:P_{org}) and total reactive P (C_{org}:P_{reac}), burial efficiencies of C_{org} and P_{org}, and inorganic carbon-to-phosphorus regeneration ratios. If P_{org} is preferentially mineralized relative to C_{org} during aerobic respiration, as many previous studies suggest, then the simulated P_{org} pool is found to be completely depleted. A modified model that incorporates the redox-dependent microbial synthesis of polyphosphates and P_{org} (termed the microbial P pump) allows preferential mineralization of the bulk P_{org} pool relative to C_{org} during both aerobic and anaerobic respiration and is consistent with the database. Results with this model show that P burial is strongly enhanced in sediments hosting fauna. Animals mix highly labile P_{org} away from the aerobic sediment layers where mineralization rates are highest, thereby mitigating diffusive PO_4^{3-} fluxes to the bottom water. They also expand the redox niche where microbial P uptake occurs. The model was applied to a hypothetical shelf setting in the early Paleozoic; a time of the first radiation of benthic fauna. Results show that even shallow bioturbation at that time may have had a significant impact on P burial; an effect that increases with subsequent deeper bioturbation. Our model provides support for a recent study that proposed that faunal radiation in ocean sediments led to enhanced P burial and, possibly, a stabilization of atmospheric O_2 levels. The results also help to explain C_{org}:P_{org} ratios in the geological record and the persistence of P_{org} in ancient marine sediments.

1. Introduction

Permanent burial of phosphorus (P) in continental margin sediments is a major control on the marine P inventory, primary productivity and possibly interglacial CO_2 concentrations (e.g. Broecker, 1982; Wallmann, 2014). On Myr time scales, P burial exerts a strong, if not dominating, influence on atmospheric O_2 levels (Van Cappellen and Ingall, 1996; Lenton and Watson, 2000; Boyle et al., 2014). Diagenetic transformations of P and the factors controlling P burial are thus intensively studied (reviewed by Benitez-Nelson, 2000; Paytan and McLaughlin, 2007; Slomp, 2011; Ruttenberg, 2014).

Particulate organic P (P_{org}) comprises more than 90 % of P that rains to the seafloor (Delaney, 1998). Phosphate (PO_4^{3-}) that is solubilized from P_{org} in the sediments can be sequestered into authigenic mineral phases, mainly as carbonate fluorapatite (CFA) and P bound or adsorbed to iron oxyhydroxides (FeP) (Berner et al., 1993). These transformations, more generally described as 'sink switching', increase the overall benthic retention efficiency of P (Ruttenberg and Berner, 1993; Anderson et al., 2001). Observations from the North Atlantic suggest that sink-switching is enhanced in sediments that are bioturbated, that is, reworked by infaunal deposit and detritus feeders (Slomp et al., 1996). The sedimentary retention capacity of P further appears to be sensitive to the ambient redox conditions (Algeo and Ingall, 2007). For example, FeP content tends to be lower under anoxic bottom waters due to reduced ferrous iron oxidation and co-sequestration of P (Sundby et al., 1992; Jensen et al., 1995; McManus et al., 1997). CFA content may be higher under these conditions, especially in modern oxygen minimum zones where phosphorites may form (Papineau, 2010).

The impact of oxygen levels on P_{org} burial is less well understood. Data on P_{org} burial efficiencies (PBE) are scarce, yet point toward lower values under anoxic versus oxic bottom waters, that is, preferential mineralization of P_{org} in anoxic settings. This trend is opposite to the organic carbon burial efficiency (CBE), which is apparently high under anoxic bottom waters and low under oxic waters (see Table 1 and further discussion by Burdige, 2007). It thus follows that molar organic carbon to phosphorus ratios (C_{org}:P_{org}) in laminated anoxic facies commonly exceed the Redfield ratio (106:1), whereas bioturbated sediments have ratios that are around Redfield or lower (Table 1). This difference is maintained, although less pronounced, for the ratio of C_{org} to reactive phosphorus (P_{reac} = P_{org} + FeP + CFA). Consistent with these findings, the inorganic carbon-to-phosphorus regeneration ratio derived from in situ flux measurements, $(C:P)_{REG}$, is often above Redfield in oxic settings and below it in sediments underlying intermittently or permanently oxygen-deficient waters (Table 1). Consequently, C:P burial ratios are used as a proxy for bottom water redox conditions and biological productivity in the paleo-ocean (Ingall and Jahnke, 1994; Slomp and Van Cappellen, 2007).

The factors that control the C_{org}:P_{org} ratio are unclear and controversial (Van Cappellen and Ingall, 1996; 1997; Colman et al., 1997). Basic questions remain, such as the extent of preferential

mineralization of P_{org} relative to C_{org} under oxic versus anoxic conditions (Colman and Holland, 2000), not least because the kinetics of C_{org} and P_{org} mineralization are very poorly understood. Some workers have proposed that microbial sequestration of P can help to explain redox-dependent C_{org}:P_{org} burial ratios (Ingall and Van Cappellen, 1990; Ingall et al., 1993; Ingall and Jahnke, 1997; Sannigrahi and Ingall, 2005; Diaz et al., 2008; Goldhammer et al., 2010; Diaz et al., 2012). Many genera of bacteria are known to accumulate and store P as polyphosphate under aerobic and nitrogenous conditions (Shapiro, 1967; Gächter and Meyer, 1993; Davelaar, 1993; Kulaev and Kulakovskaya, 2000). Polyphosphates are long chains of orthophosphate units linked by high energy phosphoanhydride bonds (Gächter and Meyer, 1993). Experimental observations indeed confirm that biologically associated P is higher in oxidized sediments (Gächter et al., 1988; Aller, 1994). It has been suggested that organic P biomolecules synthesized under oxic conditions, possibly via polyphosphate intermediates, are converted into nearly non-metabolizable organic P such as some phosphate esters and phosphonates that are subsequently permanently buried (Ingall et al., 1990; Berner et al., 1993; Ingall et al., 1993; Ingall and Jahnke, 1994; Van Cappellen and Ingall, 1994; Ingall and Jahnke, 1997). This would constitute a microbially-mediated P sink that is more efficient under oxic bottom waters, favoring an increase in P_{org} burial relative to C_{org} (i.e. low C_{org}:P_{org} burial ratios, Table 1). Refractive microbial P compounds could also help to explain the puzzling persistence of P_{org} in ancient marine sediments (Ruttenberg, 2014).

In this study, we aim to unify these different perspectives of P cycling using a diagenetic model for continental margin sediments, specifically, a shallow marine shelf with a water depth of ~100 m. The observational database in Table 1 is used to (i) ascertain the extent of preferential mineralization of P_{org} relative to C_{org} in oxic and anoxic sediments, and (ii) quantify the impact of sediment mixing by animals on P burial. Both of these are open questions with an important bearing on the interpretation of the sedimentary record.

Our interest in the role of fauna on P burial stems from the radiation of deposit feeders and burrowers in the terminal Ediacaran to early Paleozoic (ca. 542 - 420 Ma). This may have occurred against a backdrop of variability in ocean redox conditions, with conceivable impacts on, and geochemical feedbacks with, the spread of early animals (Canfield et al., 2007; Shen et al., 2008; Butterfield, 2009; Johnston et al., 2012; Lyons et al., 2012; Och and Shields-Zhou, 2012). One possible feedback loop relates to the argument that the onset of bioturbation at this time led to enhanced burial of P and stabilization of atmospheric O_2 levels (Boyle et al., 2014). The major control on sedimentary P burial in global models of ancient oceans is traditionally assumed to be the O_2 availability rather than bioturbation per se, with any mechanistic linkage with bioturbation being merely implicit (Van Cappellen and Ingall, 1994; 1996; Lenton and Watson, 2000). The validity of this assumption is tested

here with the diagenetic model. We find that indwelling fauna, in combination with microbial P synthesis, would have strongly enhanced P burial in the early Palaeozoic Era.

2. Model

2.1. Architecture and application

A vertically-resolved 1-D model is used to investigate the coupled biogeochemical cycling of C, N, P, Mn, Fe and S in the uppermost meter of fine-grained continental shelf sediments (ca. 100 m water depth). Full details of the model can be found in the Supplementary Material and in Dale et al. (2015a). For the present study, we limit the biogeochemical model description to the previously unpublished P cycle. Key model boundary conditions and parameters are listed in Table 2.

A total of 13 solutes and 17 solid species are considered in the model. Particulate matter is transported dynamically through the sediment column by accumulation (burial) and bioturbation. Solutes are transported by molecular diffusion and bioirrigation. The coupling of biogeochemistry and transport is summarized by the following generic mass-conservation equations (Berner, 1980; Boudreau, 1997):

$$\varphi \frac{\partial C_a}{\partial t} = \frac{\partial}{\partial z}\left(\varphi D \frac{\partial C_a(z,t)}{\partial z}\right) - \frac{\partial \varphi(L)\omega_{acc} C_a}{\partial z} + \alpha(0)\cdot\gamma\cdot\exp\left(-\frac{z}{z_{bio}}\right)\varphi(C_a(0) - \mathrm{C_a}) + \Sigma\varphi R \quad (1a)$$

$$(1-\varphi)\frac{\partial \mathrm{C_s}}{\partial t} = \frac{\partial}{\partial z}\left((1-\varphi)D_b(0)\cdot\exp\left(-\frac{z^2}{2\cdot {z_{bt}}^2}\right)\frac{\partial C_s}{\partial z}\right) - \frac{\partial\left(1-\varphi(L)\right)\cdot\omega_{acc}\cdot C_s}{\partial z} + \Sigma(1-\varphi)R \quad (1b)$$

where C_a and C_s are the time- and depth-dependent concentrations of solutes in mmol cm^{-3} (of pore water) and particulate species in weight percent of dry sediment (%), respectively, z (cm) denotes depth in the sediment, φ is porosity, ω_{acc} (cm yr^{-1}) is the sedimentation rate, D (cm^2 yr^{-1}) is the molecular diffusion coefficient, and ΣR is the sum of the rate of change of concentration due to biogeochemical reactions. Constitutive equations describing the depth dependency of transport parameters are provided in Table S1, and the complete list of biogeochemical reactions, rate expressions and parameters are given in Table S2 to S5. In this study, model results represent steady state simulations, that is, where concentrations are invariable with time (∂C/∂t = 0).

The third term on the right-hand-side of Eq. (1a) describes the exponential decrease of bioirrigation with sediment depth. Bioirrigation is the non-local exchange of seawater with burrow water by the pumping activity of tube-dwelling animals (Aller and Aller, 1992). Mathematically, the process is described using the parameters $\alpha(0)$ (y^{-1}) and $C_a(0)$, which are the maximum bioirrigation coefficient

(under oxic bottom waters) and solute concentration at the sediment-water interface, respectively. z_{bio} (cm) is the attenuation coefficient that parameterizes the depth to which burrows extend below the sediment surface. The dimensionless parameter γ is a scaling parameter for ferrous iron to reflect rapid oxidation on burrow walls (see Dale et al., 2015a).

Bioturbation, the first term on the right-hand-side of Eq. (1b), is treated as biodiffusion, analogous to molecular diffusion, using a Gaussian function to describe the decrease in sediment mixing with sediment depth (Boudreau, 1996). The maximum rate of particle reworking in the surface mixed layer is defined by the bioturbation enhanced diffusion coefficient, $D_b(0)$ ($cm^2\ yr^{-1}$). The parameter z_{bt} (cm) defines the depth at which bioturbation intensity is half of $D_b(0)$, according to the Gaussian decrease in bioturbation intensity. A relation between $D_b(0)$ and z_{bt} has, to our knowledge, not been demonstrated empirically, and these parameters are independent of one another.

Our treatment of biodiffusion can be viewed as reverse conveyor-belt feeding, i.e. downward transport of particles (reviewed by Burdige, 2006; Meysman et al., 2003). It is also a local process, because it mixes sediment between adjacent layers. However, under natural conditions, most modes of sediment transport adhere to non-local exchange formalisms, that is, transport of material between non-adjacent sediment layers (Meysman et al., 2003). Non-local sediment mixing can occur both upwards by conveyor-belt (head-down) feeding and downwards (e.g. ingestion at surface, egestion at depth). Non-local conveyor-belt feeding tends to retain radiotracers such as ^{210}Pb in the surface mixed layer, and steady-state tracer profiles resulting from this type of transport tend to resemble those resulting from the biodiffusion model (Boudreau, 1986). Non-local reverse conveyor-belt feeding, on the other hand, gives rise to subsurface maxima in tracer profiles (Smith et al., 1986). Although the exact pattern of tracer distribution will depend on the specific mixing mechanism, each type of feeding behavior will lead to a mixing of aged and fresh organic matter within the bioturbated. In this paper, we adopt the biodiffusion model because it has been proven to be a robust empirical model for sediment mixing and is straightforward to solve numerically. More complex treatments have been developed elsewhere (Robbins, 1986; Boudreau, 1986).

The value of z_{bt} is set to 3 cm, to reflect a mean mixed layer thickness in the modern ocean of 5 to 10 cm (Boudreau, 1997; Teal et al., 2008). The parameters z_{bt} and z_{bio} are deemed to be independent of one another since the ecology of sediment 'bulldozers' and irrigators is different. Here, we simply set z_{bio} to 2 cm so that the irrigation depth is similar to the bioturbation depth (Archer et al., 2002). It is important to note that these parameters correspond to the sediment mixed layer where reworking or bulldozing by animals is sufficiently intense to homogenize the sediment (Tarhan et al., 2015). In contrast, burrows may extend many decimeters below the mixed layer and impact biogeochemical cycling there. The ghost shrimp *N. californiensis*, for example, can enhance denitrification by pumping seawater nitrate into deep sediment layers (Bertics et al., 2010). In this paper, we do not

consider deep irrigation because it is in all likelihood much weaker than surface irrigation (Fossing et al., 2000). Our focus on the surface sediment will facilitate comparisons with the early Paleozoic scenarios where the maximum burrow depth is limited to a few cm (Tarhan et al., 2015). The sensitivity of the model to bioturbation and bioirrigation is tested later.

The model is applied across a range of bottom water dissolved O_2 concentrations from anoxic (0.1 μM) to oxic (150 μM). The former threshold is not strictly anoxic, but instead represents the micro-aerobic conditions that exist within some 'anoxic' oxygen minimum zones such as in the Eastern South Pacific Ocean (Thamdrup et al., 2012). Under oxic conditions, the parameters $D_b(0)$ and $\alpha(0)$ take values of 28 cm^2 yr^{-1} and 465 y^{-1}, respectively (Supplement). They are allowed to decrease gradually toward zero if O_2 drops below a 20 μM threshold. At this concentration, a decrease in species richness and bioirrigation has been observed (Levin and Gage, 1998; Dale et al., 2013) with surface deposit feeders dominating over burrowing macrofauna (Middelburg and Levin, 2009).

We begin by focusing on modern sediments, for which data are relatively abundant, in order to parameterize the P cycle. To avoid the risk of being too site-specific, P turnover is mainly constrained by the data in Table 1 that originate from a wide range of marine settings. In that sense, the model is more emblematic of an average shallow continental margin setting. Parameterization of transport and biogeochemical processes draws from a large body of previous empirical studies from shelf environments (Supplementary Material). In particular, this includes realistic organic matter and iron fluxes to the seafloor, organic matter reactivity, reaction rate constants, sedimentation rates, and bioturbation and bioirrigation intensities. Most of these are taken directly from the shelf scenario in Dale et al. (2015a) that is confirmed against a global database of dissolved iron fluxes. Only a minimal amount of additional parameter tuning has been used for organic matter degradation as described below. The model is then applied to the early Paleozoic shelf environment (ca. 542 – 420 Ma) by altering the boundary conditions accordingly. We define sediments underlying anoxic waters as 'anoxic' whereas bioturbated sediments under oxic waters are termed 'oxic', whilst noting that the latter quickly turn anoxic and anaerobic below the thin surface oxidized layer (< ca. 1 cm, Glud et al., 2008 and Results).

2.2. Phosphorus biogeochemistry

The P cycle initially centers on three particulate species (Fig. 1): organic P (P_{org}), iron-associated P (FeP) and carbonate fluorapatite (CFA). Dissolved P takes the form of inorganic orthophosphate (PO_4^{3-}). The P model is similar to previous applications (Van Cappellen and Berner, 1988; Reed et al., 2011; Kraal et al., 2012) and, like these other models, highly simplifies the representation of P cycling in sediments, especially with regard to authigenic P mineral formation. However, the main diagenetic

pathways are included. Our model structure differs from the other studies by the inclusion of P uptake by microorganisms (Section 3.3), plus a more realistic description of organic matter degradation kinetics. P concentrations are reported in μmol g^{-1} of P (0.01 wt. % = 3.23 μmol g^{-1}).

Mineralization of deposited organic matter, chemically defined as $CN_{rNC}P_{rPC}$, drives all diagenetic reactions that take place in the model. Parameters r_{NC} and r_{PC} are the (Redfield) atomic ratios of particulate organic nitrogen and phosphorus to carbon (Table 2). Dissolution of organic nitrogen and phosphorus is coupled to the rate of C_{org} mineralization. C_{org} is oxidized by several pathways; aerobic respiration, nitrate and nitrite reduction (denitrification), manganese oxide reduction, dissimilatory iron reduction, sulfate reduction and methanogenesis in that order (R_1 to R_7, Table S4). The kinetics of C_{org} mineralization is described using continuum kinetics, where the rate constant for C_{org} degradation is time dependent (Middelburg, 1989; Boudreau and Ruddick, 1991):

$$k(t) = \upsilon\,(a + t)^{-1} \quad (2)$$

In this expression, a (yr) is the average lifetime of the reactive components and υ (dimensionless) is the distribution of C_{org} reactivity. Low υ values indicate that C_{org} is dominated by refractory components, whereas higher values correspond to a more even distribution of reactive types. Similarly, C_{org} characterized by low a will be rapidly degraded whereas high a implies less reactive material that is more likely to be buried to deeper sediments. Reactive continuum-type models predict a more realistic profile of C_{org} reactivity with sediment depth than those based on 'multi-G' kinetics. The latter require a somewhat arbitrary number of discrete C_{org} fractions, or 'G', to be assigned individual rate constants that are poorly defined at the global scale (Boudreau and Ruddick, 1991). The choice of degradation kinetics is important because it determines the sediment redox structure and the depth at which P fractions are dissolved or precipitated and, hence, phosphate fluxes across the sediment-water interface. However, continuum models are difficult to apply to bioturbated sediments since the age and reactivity of organic matter within the bioturbated zone tend to be poorly constrained (Boudreau and Ruddick, 1991; Middelburg, 1989). Ages of radioactive tracers within the bioturbated zone depend not only on the burial velocity and bioturbation rate but also on the decay rate of the tracer itself (Meile and Van Cappellen, 2005).

We used a previous approach (Dale et al., 2015a) that calculates discrete C_{org} fractions from the continuum parameters a and υ that, when summed together, give the same C_{org} reactivity profile as the continuum model. More accurate results are produced as the number of defined C_{org} fractions increases. Fourteen fractions were found to give an excellent agreement with the continuum model (Dale et al., 2015a), using an initial parameterization of a (3×10^{-4} yr) and υ (0.125) constrained from oxic degradation experiments with fresh phytoplankton (Boudreau et al., 2008). The rate of P_{org} mineralization for each pathway is initially determined as:

$$R_{P_{org}} = r_{CP} \cdot \mathrm{RPOC} \cdot \psi \quad (3)$$

where RPOC is the total rate of POC degradation and ψ represents the sum of oxidant limitation and inhibition terms (see Supplement). Later, the rate of P_{org} mineralization will be adjusted depending on whether organic matter is respired aerobically or anaerobically. Organic phosphorus is mineralized to dissolved PO_4^{3-}.

Four reactive fractions of particulate iron oxides were defined according to the classification scheme based on wet chemical extractions (Canfield et al., 1992; Poulton et al., 2004). These are defined as highly reactive (Fe_{HR}, e.g. nano-geothite), moderately reactive (Fe_{MR}, e.g. goethite and hematite), and poorly reactive (Fe_{PR}, e.g. iron silicates). Fe_{HR}, Fe_{MR} and Fe_{PR} are all dissolvable by sulfide, but at different rates (see Supplementary Material). The model also includes detrital (unreactive) iron.

Reactions that couple the Fe and P cycle are the dissolution of Fe_{HR} by dissimilatory iron reduction (R_5), authigenic precipitation of Fe_{HR} via aerobic and anaerobic oxidation of ferrous iron (R_{13}, R_{14}, R_{24}), reductive dissolution of Fe_{HR} and Fe_{MR} by sulfide (R_{26}), and the ageing and crystallization of Fe_{HR} into more stable Fe_{MR} phases (R_{28}). These are given as (see Supplement for more details):

R_5: $CN_{rNC}P_{rPC} + 4Fe_{HR} + 4\theta_{HR} \rightarrow 4Fe^{2+} + TCO_2 + r_{NC}NH_4^+ + (4\theta_{HR} + r_{PC})\, PO_4^{3-}$ (4)

R_{13}: $Fe^{2+} + 0.25O_2 + 1/\varepsilon_{aut} \cdot PO_4^{3-} \rightarrow Fe_{HR} + 1/\varepsilon_{aut} \cdot FeP_{HR}$ (5)

R_{14}: $Fe^{2+} + 0.2NO_3^- + 1/\varepsilon_{aut} \cdot PO_4^{3-} \rightarrow 0.1N_2 + Fe_{HR} + 1/\varepsilon_{aut} \cdot FeP_{HR}$ (6)

R_{24}: $Fe^{2+} + Mn_j + 1/\varepsilon_{aut} \cdot PO_4^{3-} \rightarrow Mn^{2+} + Fe_{HR} + 1/\varepsilon_{aut} \cdot FeP_{HR}$ for j = HR, MR (7)

R_{26}: $Fe_j + \theta_j + 0.5H_2S \rightarrow Fe^{2+} + 0.5S^0 + \theta_j PO_4^{3-}$ for j = HR, MR (8)

R_{28}: $Fe_{HR} + \theta_{HR} + 1/\varepsilon_{age} \cdot PO_4^{3-} \rightarrow Fe_{MR} + \theta_{HR}PO_4^{3-} + 1/\varepsilon_{age} \cdot FeP_{MR}$ (9)

Detrital P bound within highly crystalline iron fractions and other minerals is not considered in the model. The iron module also includes precipitation of iron sulfide minerals, although without associated P turnover (Krom and Berner, 1980).

The change in FeP content is calculated using the particulate fraction of P to Fe (θ, mol P / mol Fe) and/or Fe:P enrichment ratios (ε, mol Fe / mol P) (Dale et al., 2013). The capacity of poorly crystalline iron oxides to sequester large amounts of ambient PO_4^{3-} is well recognized (Torrent et al., 1992; Slomp et al., 1996; Anschutz et al., 1998; Feely et al., 1998). The Fe:P ratio in amorphous iron oxides in surface sediments, principally nano-particulate goethite, seems to be constant at around 10

(Sundby et al., 1992; Jensen and Thamdrup, 1993; Slomp et al., 1996; Anschutz et al., 1998; van der Zee et al., 2003). Hence, we take this value for ε_{aut} in R_{13}, R_{14} and R_{24}. The rate expressions for these reactions include a rate–limiting term that slows down the rate of PO_4^{3-} uptake into Fe_{HR} if PO_4^{3-} concentrations are diminished to low levels (Table S5). Authigenic Fe_{HR} can therefore have a Fe:P ratio that is higher than 10 if the ambient PO_4^{3-} concentration is very low at the site where Fe^{2+} crystallizes from solution.

The FeP pool can be preserved by ageing processes (Lijklema, 1980; Borggaard, 1991). However, crystallization decreases the mineral surface area and the sorptive capacity of PO_4^{3-}, releasing PO_4^{3-} to solution (Houben, 2003). Based on observations by Poulton and Canfield (2006), the Fe:P ratio of recrystallized iron, ε_{age}, is set to be a factor of 4 higher than for the highly reactive fractions (40).

The only allochthonous source of FeP is associated with the flux of Fe_{HR}, which requires knowledge of the Fe:P atomic ratio in iron oxides deposited on the shelf (ε_{all}). Most reactive iron oxide deposited there originates as colloidal coagulates formed in the low salinity region in estuaries (Boyle et al., 1977). The fraction of P that is adsorbed to these colloids decreases with increasing salinity, pH and decreasing concentrations of suspended particulate matter (Boyle et al., 1977; Bale and Morris, 1981; Lebo, 1991; Spiteri et al., 2008). Jordan et al. (2008) reported an increase in the Fe:P ratio in the Patuxent River estuary from ca. 9 in the freshwater end member to ca. 13 at a salinity of 7. Measurements in the St. Lawrence Estuary show a Fe:P ratio of around 18 to 23 close to the sea water end member (Lucotte and D'Anglejan, 1983). Further P depletion in iron oxides can occur if the suspended material has first been subjected to reductive dissolution in the estuarine sediment (Berner and Rao, 1994). These studies demonstrate a wide range of the Fe:P ratio in deposited iron oxides. For our model we assume that $\varepsilon_{all} = 25$, that is, depleted in P relative to authigenic Fe_{HR}.

Finally, the model includes the irreversible crystallization of dispersed CFA directly from porewater PO_4^{3-} without a precursor phase (Froelich et al., 1988; Van Cappellen and Berner, 1988). We assume the following idealized stoichiometry (Froelich et al., 1988):

$$10Ca^{2+} + (6-x)PO_4^{3-} + xCO_3^{2-} + (2+x)F^- \rightarrow Ca_{10}(PO_4)_{6-x}(CO_3)_xF_{2+x} \quad (10)$$

where a value of $x = 0.26$ is assigned, such that the F:P ratio in the crystallized apatite is 0.39 (Froelich et al., 1988; Van Cappellen and Berner, 1988). Changes in the extent of substitution of carbonate and fluoride due to factors such as the pore fluid composition are ignored (Froelich et al., 1988). The rate of apatite precipitation is described as a kinetically-controlled process. The rate limiting factor is the concentration of PO_4^{3-} in excess of the concentration in thermodynamic equilibrium with CFA, C_{eq} (Van Cappellen and Berner, 1988). Apatite formation is inhibited if $PO_4^{3-} < C_{eq}$; taken as 10 µM (Van Cappellen and Berner, 1988). This assumes that the PO_4^{3-} concentration is the limiting factor for CFA precipitation rather than Ca^{2+} or F^-, which is reasonable since apatite is

more enriched in P than F, and seawater Ca^{2+} concentrations are orders-of-magnitude higher (Froelich et al., 1983; Schuffert et al., 1994). A limiting term for F^- is nonetheless included in the rate expression to ensure that CFA cannot crystallize if F^- is completely consumed (Table S5). The rate constant for CFA precipitation is assigned to be 1 yr^{-1} based on studies in Arabian Sea sediments (Kraal et al., 2012). A more rigorous expression for CFA precipitation that considers the effect of porewater pH and carbonate content should be explored in future work (Jahnke et al., 1983).

The depositional flux of apatite to the seafloor is set to zero (Table 2). We have chosen to omit detrital apatite from the model since it is believed to be unreactive (Berner et al., 1993). Vivianite precipitation is also not considered since this mineral is likely to be undersaturated in margin sediments (see Supplement). Estimates of the contribution by biogenic P (typically in the form of CFA fish bones and scales) to porewater dissolved P in sediments are scarce. Stoichiometric porewater models suggest that biogenic P contributes insignificantly to PO_4^{3-} turnover in sediments outside of upwelling areas (Suess, 1981). Froelich et al. (1982) also calculated that burial of biogenic fish debris is a minor sink for P at the global scale. The fact that global fish production (ca. 2.5 g m^{-2} yr^{-1}, Jennings et al., 2008) is equivalent to less than 2 % of primary production (ca. 150 g m^{-2} yr^{-1}, Sarmiento and Gruber, 2006) seems to support this idea. For these reasons, biogenic P is considered to be inconsequential and is not included in the model (Froelich et al., 1982). Nonetheless, more work is needed to properly determine the importance of biogenically-derived P to benthic P fluxes.

3. Parameterization of the phosphorus model

3.1. C_{org} and P_{org} mineralization

A mechanistic understanding of P burial in sediments first requires a careful analysis of the poorly understood kinetics of P_{org} mineralization. Since P_{org} burial is often discussed in terms of C_{org}:P_{org} ratios, the first step in the modelling procedure was to constrain the mineralization of C_{org} using the available database of organic carbon burial efficiencies (CBE) (Table 1).

The CBE in sediments on the continental margin under oxic bottom waters is 25 ± 15 % (Table 1) versus >40 % for oxygen-deficient bottom waters (O_2 < 20 μM). This difference has been argued to be driven by preferential preservation of C_{org} in the absence of oxygen (Demaison and Moore, 1980; Hartnett et al., 1998; Hedges et al., 1999). Running the anoxic model with C_{org} mineralization defined using the degradation kinetics for fresh phytoplankton (see *2. Methods*) predicts a low CBE of 15 %. These kinetics thus over-predict C_{org} mineralization in natural anoxic sediments, probably because the experiments made no allowance for anaerobic mineralization (Westrich and Berner, 1984). The model was therefore adjusted by decreasing the value of the parameter describing the C_{org} reactivity

distribution, υ, from 0.125 to 0.05, implying a greater fraction of less degradable components within the bulk organic mixture. Re-running the model gives a CBE of 47% for both anoxic and oxic sediments. Whilst this agrees with observations in anoxic sediments (Table 1), the predicted CBE in oxic (bioturbated and bioirrigated) sediments is too high. Enhanced C_{org} degradation under oxic bottom waters was thus achieved by multiplying the rate of aerobic C_{org} degradation by an acceleration factor, *foxC* (see Table S5). With *foxC* = 2, for example, the model predicts a more realistic CBE of 16% for oxic sediments. This adjustment fits with the long-standing paradigm of preferential mineralization under oxic conditions (Hartnett et al., 1998; Hedges et al., 1999).

PBE is lowest in sediments underlying oxygen deficient bottom waters, with values in the range of 2 to 11 % (Table 1). To achieve this with the model, it was necessary to enhance the dissolution of P_{org} during anaerobic respiration *relative* to C_{org} using an acceleration factor, *fanoxP* (Table S5). A value of 1.7 provides a PBE of 12 % for the anoxic scenario that is in good agreement with previous studies with bottom water O_2 < 20 μM. The corresponding regeneration ratio, $(C:P)_{REG}$, is 64, that is, P-enriched relative to the Redfield ratio of the organic matter raining to the seafloor. This also agrees with measured $(C:P)_{REG}$ of around 10-60 for anoxic margins (Table 1). Furthermore, the C_{org}:P_{org} burial ratio is 423, again well within the range of the observations (300 - 600).

If an equivalent acceleration factor of 1.7 is used for P_{org} mineralization relative to C_{org} during aerobic respiration (*foxP*), then P_{org} degradation is too high and the sediment loses too much PO_4^{3-} by diffusion to the water column. The result is a PBE of only 5% and a C_{org}:P_{org} burial ratio of 335. PBE estimates for sediments under oxic bottom waters are scarce, and probably in the region of ca. 20 to 40 %, whilst burial ratios range from 30 to 115 (Table 1). Therefore, *foxP* must be less than *fanoxP* for the current model set-up. With *foxP* = 0.5, that is, slower than the rate of aerobic C_{org} mineralization, the model predicts a PBE of 33% and a C_{org}:P_{org} burial ratio of 53 for oxic sediments, respectively, both of which are supported by measured data. Furthermore, $(C:P)_{REG}$ is 140, not dissimilar to observations under oxic bottom waters of 118 ± 24 (Wallmann, 2010).

3.2. Preferential mineralization of P_{org} versus C_{org}

To summarize, the model can reproduce PBEs, $(C:P)_{REG}$ and C_{org}:P_{org} burial ratios that are within the ranges of the field data if P_{org} mineralization proceeds at roughly half the rate of C_{org} mineralization during aerobic respiration and twice as fast during anaerobic respiration. In that case, we should expect to see C_{org}:P_{org} ratios in oxic environments that are P enriched relative to Redfield (<< 106:1). However, field data rather indicate that P_{org} is mineralized preferentially to C_{org} under oxic conditions. For instance, the molecular composition of particulate P sinking through oxic water columns down to ca. 4000 m in diverse oceanic settings has been analyzed using ^{31}P NMR (nuclear magnetic

386 resonance) spectroscopy and sequential extractions (Paytan et al., 2003; Faul et al., 2005). These
387 studies showed that phosphate diesters are preferentially solubilized, with C_{org}:P_{org} ratios ranging from
388 276 to 1138 and a mean value of 318. Selective P remineralization also occurs in the dissolved
389 organic fraction. Clark et al. (1998) measured an increase in the C:P ratio of dissolved organic matter
390 with depth in the Pacific Ocean from 247:1 at the surface to 539:1 at 4000 m. Further examples of
391 preferential mineralization of P_{org} in oxic waters have been discussed by Ruttenberg (2014). The
392 current model formulation of aerobic mineralization is thus inconsistent with the observations in the
393 water column.

394 Although temporal and spatial variability of water column particle fluxes creates uncertainty in the
395 data analysis (e.g. Paytan et al., 2003), it seems reasonable to assume that preferential mineralization
396 of P_{org} relative to C_{org} continues in oxidized surface sediments. Identification of preferential P_{org}
397 mineralization in sediments is more problematic because the thickness of the diffusive oxic layer at
398 the sediment-water interface is typically only a few mm thick (Glud et al., 2008). Furthermore, P_{org}
399 dynamics are overprinted by inorganic P cycling and sediment reworking and mixing by bioturbation.
400 Diagenetic models can help to eliminate such interferences. Using such an approach, Krom and
401 Berner (1981) inferred preferential loss of P_{org} in surface sediments in Long-Island Sound by
402 comparing the calculated C_{org}:P_{org} stoichiometry of mineralized organic matter versus the bulk
403 C_{org}:P_{org} composition of the phytoplankton community. They further showed that P_{org} mineralization
404 in the oxic layer was more rapid than in the underlying anoxic sediments. The empirical model
405 developed by Ingall and Van Cappellen (1990) also required preferential regeneration of P_{org} to
406 simulate C_{org}:P_{org} burial ratios in a wide range of marine environments. In contrast, Reed et al. (2011)
407 reported opposite trends for P turnover in a modern (seasonally) hypoxic basin. They tuned their
408 model to data assuming selective P_{org} mineralization relative to C_{org} under anoxic conditions only.

409 Despite the ambiguity that exists concerning the extent of preferential mineralization of P_{org} relative to
410 C_{org} under oxic conditions (Ruttenberg, 2014), the consensus seems to be that P_{org} is mineralized more
411 rapidly than C_{org} during the initial stages of mineralization, and certainly not more slowly.
412 Consequently, if P_{org} is indeed preferentially degraded in oxic sediments, then the PO_4^{3-} that is
413 released close to the sediment water interface must be sequestered and entrained in the sediment
414 before it can escape to the water column. Constraints provided by C_{org}:P_{org} burial ratios and PBE
415 strongly indicate that this sink is organic in nature.

416

417 *3.3. Expanding the model: P sequestration by microorganisms*

418 The model is extended to include a simple microbial P cycle (Fig. 1) to investigate whether the
419 hypothesized authigenic synthesis of refractive biomolecules (see Introduction) can explain

preferential mineralization of P_{org} relative to C_{org} and the observed C:P burial ratios in different marine settings. Two additional species are considered; polyphosphate (P_{poly}) and unreactive microbial organic P ($P_{org\text{-}U}$). The microorganisms are not modeled explicitly, and P_{poly} and $P_{org\text{-}U}$ are assumed to be particulate species transported passively through the sediments by bioturbation and burial. A deposition flux of zero is prescribed at the sediment surface for P_{poly} and $P_{org\text{-}U}$ (Robin boundary), with a zero gradient at the bottom (Neumann boundary).

Microorganisms assimilate porewater PO_4^{3-} in aerobic and nitrogenous sediments leading to an increase in the P_{poly} pool (Davelaar, 1993). A fraction (f_{poly}) of P_{poly} is converted to $P_{org\text{-}U}$ to simulate the synthesis of refractive P biomolecules. This fraction is buried without further reaction and constitutes a microbial P pump that removes bioavailable P from the ocean. The remainder ($1 - f_{poly}$) is recycled back to the bulk P_{org} pool on the understanding that labile dead bacterial biomass is remineralized. P_{poly} that is transported into anaerobic sediment layers is rapidly hydrolyzed back to PO_4^{3-}. This simulates the breakdown of P_{poly} by bacteria to gain energy to survive anaerobiosis as well as the lack of P_{poly} in anoxic sediments (Gächter and Meyer, 1993; Davelaar, 1993; Sannigrahi and Ingall, 2005; Schulz and Schulz, 2005; Brock and Schulz-Vogt, 2010). Phosphate that is released to the porewater can be trapped in authigenic phases (sink switching) or diffuse upwards and re-assimilated by bacteria as P_{poly}. Transformation of P_{poly} into CFA is not considered (Diaz et al., 2008), although we recognize that this may take place in oxygen minimum zones (Goldhammer et al., 2010).

The proposed cycle is by necessity highly simplified since the distribution of different classes of organically-bound P molecules in sediments is not well understood and polyphosphates are typically extracted in operationally defined P_{org} pools (Sannigrahi and Ingall, 2005; Diaz et al., 2012). X-ray spectromicroscopy has nonetheless revealed that polyphosphates are an important P phase at oxic-anoxic interfaces in marine sediments, and that they may constitute a larger fraction of the operationally-defined detrital P than previously assumed (Diaz et al., 2008; Kraal et al., 2015). With this in mind, the following equation describing the rate of change of P_{poly} in the sediment is proposed:

$$\frac{dP_{poly}}{dt} = + \text{synthesis} - \text{hydrolysis} - P_{org\text{-}U}\ \text{synthesis} - P_{org}\ \text{synthesis} \quad (11)$$

The kinetics and parameterization of these pathways are only vaguely constrainable by field and experimental observations. We make the assumption that the rate of P_{poly} synthesis (R_{30}) is dependent on the concentration of PO_4^{3-} in the porewater as well as the concentration of NO_X ($NO_3^- + NO_2^-$):

$$R_{30} = k_{30} \cdot PO_4^{3-} \cdot NO_X \quad (12)$$

where k_{30} is the rate constant. No dependency on O_2 is included because it is exhausted before NO_X, such that the sediment penetration depth of NO_X is higher than for O_2 (discussed below). The impact of C limitation on P_{poly} synthesis is not considered (Steenbergh et al., 2012).

Hydrolysis of P_{poly} is defined using a dimensionless oxygen threshold, δ:

$$R_{31} = k_{31} \cdot P_{poly} \cdot \delta \quad (13)$$

where $\delta = 0$ for $O_2 \geq 1$ µM and $\delta = 1$ for $O_2 < 1$ µM. Transformation of P_{poly} to P_{org} (R_{32}) and $P_{org\text{-}U}$ (R_{33}) are described as first-order processes:

$$R_{32} = k_{32} \cdot (1 - f_{poly}) \cdot P_{poly} \quad (14)$$

$$R_{33} = k_{33} \cdot f_{poly} \cdot P_{poly} \quad (15)$$

The rate coefficients k_{31} to k_{33} are set to high values of 50 yr^{-1}. Rapid turnover of P_{poly} has been inferred from the transient development of large subsurface PO_4^{3-} peaks attributed to the breakdown of bacterial P_{poly} (Schulz and Schulz, 2005; Dale et al., 2013). The rate limiting step in the microbial P cycle is P_{poly} synthesis, such that the turnover of microbial P pump can be regulated by adjusting k_{30} whereas the fraction channeled into refractive $P_{org\text{-}U}$ is determined by f_{poly}. Fast transformation of PO_4^{3-} into P_{poly} by sulfur oxidizing bacteria has been measured using ^{33}P tracer (Goldhammer et al., 2010). We acknowledge the possibility, and likelihood, that a different set of parameters or microbial P cycling pathways could lead to equivalent results. Our main interest here is whether P_{org} synthesis by bacteria is a concept that is supported by the data.

On the understanding that aerobic P_{org} mineralization is more rapid than C_{org} mineralization, we initially set *foxP*, the enhancement of aerobic P_{org} mineralization relative to C_{org}, equal to 2. We then adjusted the rate of P_{poly} synthesis to bring the model back into the range of the observations.

4. Results

The model with the microbial P pump is able to simulate the entire suite of field observations in oxic and anoxic sediments with $k_{30} = 3 \times 10^7$ M^{-1} yr^{-1} and a slightly higher *fanoxP* of 2 (Table 2 and 3). The latter adjustment from the previous value of 1.7 compensates for the limited amount of microbial P_{org} that is synthesized in the nitrogenous layer in the anoxic sediment. Furthermore, f_{poly} is equal to 0.25, such that 25 % of the P_{poly} pool that is not hydrolyzed is converted to $P_{org\text{-}U}$ and 75 % to P_{org}. The relative fractionation of P_{poly} into labile and unreactive P_{org} depends somewhat on the poorly constrained values of *foxP*. Whilst there is obviously some latitude in these numbers, we note that the model would not be able to simulate the database if P_{poly} were entirely converted to P_{org} or $P_{org\text{-}U}$ alone. An important conclusion from this model set-up is that P_{org} is preferentially mineralized relative to C_{org} during aerobic *and* anaerobic respiration.

The mass fluxes in Fig. 2 show that P turnover is more intense in oxic sediments. P_{org} mineralization rates are 136 μmol m^{-2} d^{-1}, versus 89 μmol m^{-2} d^{-1} in anoxic sediments. This is partly compensated by higher rates of PO_4^{3-} sequestration into P_{poly} (82 versus 19 μmol m^{-2} d^{-1}). By way of comparison, measured P sequestration rates by sulfur oxidizing bacteria are of a similar magnitude (210 to 780 μmol m^{-2} d^{-1}; Goldhammer et al., 2010). As a result, PO_4^{3-} concentrations are lower in oxic sediments and P_{org} and P_{reac} concentrations are higher (green and black curves, Fig. 3). Identical qualitative trends have been observed at neighboring oxic and anoxic sites in Effingham Inlet (Ingall et al., 2005; Sannigrahi and Ingall, 2005). Removing the microbial P pump leads to complete dissolution of P_{org} in oxic sediments and low accumulation of other authigenic P phases (red curves, Fig. 3).

5. Discussion

5.1. P cycling with the microbial P pump

The simulated P dynamics considering microbial P sequestration and burial are consistent with the observed burial efficiencies, benthic fluxes and burial ratios in diverse marine settings, and suggest an important microbial control of P cycling in sediments. Permanent microbial P sequestration can be viewed as a sink-switching mechanism that permits preferential burial of P relative to C_{org} (Ruttenberg and Berner, 1993; Filippelli and Delaney, 1996; Anderson et al., 2001). Microorganisms may, therefore, act as a barrier to PO_4^{3-} fluxes in the same way as P sequestration by iron oxides and apatite crystallization (Sundby et al., 1992; Gächter and Meyer, 1993; Anschutz et al., 1998; Slomp et al., 1996; Sannigrahi and Ingall, 2005). Microbial sink-switching leads to C_{org}:P_{reac} burial ratios of 44 and 196 in oxic and anoxic sediments, respectively (Table 3). These agree well with those measured above and within Mediterranean sapropels (21 versus 54 - 161; Slomp et al., 2004) and with values of 140 ± 50 and 180 ± 90 from (anoxic) black shale sequences from the Cayuga Basin and Yorkshire coast (Ingall et al., 1993; Anderson et al., 2001).

In the current oxic configuration, PO_4^{3-} trapping into iron oxides (ca. 9 μmol m^{-2} d^{-1}; Fig. 2) removes a relatively small fraction of PO_4^{3-} from the porewater compared to microbial P. This result arises from tuning the model to the observational database in Table 1, and involves no tweaking of other parameters to lessen the importance of Fe-P cycling. The iron cycle has been previously constrained from a global empirical database (Dale et al., 2015a). A lesser contribution (quantitatively speaking) of iron-associated P cycling on P burial relative to P_{org} is consistent with previous findings from some settings (Ruttenberg and Berner, 1997; Ingall and Jahnke, 1997; Sannigrahi and Ingall, 2005) but not others (Jensen et al., 1995; Slomp et al., 1996). This can be attributed potentially to numerous factors, such as regional variability in external iron inputs, bottom water O_2 levels, and bioirrigation and bioturbation intensities. Model sensitivity analysis (not shown) reveals that the fraction of P that is

buried in association with iron oxides is particularly sensitive to the Fe:P molar ratio in the iron fraction of Fe_{MR} that is crystallized from Fe_{HR} by ageing (ε_{age}). This ratio is set to 40, compared to a molar ratio of 10 for freshly precipitated Fe_{HR}. The higher value represents an increase in the crystallinity of Fe_{MR} relative to Fe_{HR} and subsequent loss of P binding sites (see *2. Model*). The rate of PO_4^{3-} that is sequestered into Fe_{MR} by ageing is proportional to ε_{age}, such that a halving of ε_{age} doubles the burial flux of P associated with Fe_{MR}. Thus, precipitation and ageing of FeP could conceivably sequester more PO_4^{3-} than currently assumed by the model. It cannot, however, explain the entire sink for PO_4^{3-} because this would be inconsistent with the C_{org}:P_{org} burial ratios and P_{org} burial efficiencies.

The fact that total P_{org} in oxic settings is roughly twice that in anoxic sediments demonstrates that recalcitrant microbial P_{org} constitutes around half of the P_{org} buried below the bioturbated layer (Fig. 3). A higher turnover of microbial biomass under oxic versus anoxic conditions has been noted before (Sun et al., 2002), and conceivably could be coupled to a more intense microbial P pump. In this study, we did not explicitly examine the C_{org}:P_{org} ratio of the microorganisms or simulate microbial C_{org}. The C_{org}:P_{org} ratio of bacteria has been often cited to be between 29 and 63 (Berner et a., 1993), which is close to the simulated ratio in oxic sediments of 73 (Table 3). Yet, X-ray microanalysis on intact cells from surface sediment samples in the Baltic Sea revealed high bacterial C_{org}:P_{org} ratios up to 400, although this may be related to substrate (C_{org}) limitation (Steenbergh et al., 2012). This type of quantitative information could serve to further validate the model if the degradation kinetics of cellular P_{org} were known, for both oxic and anoxic sediments. Compared to FeP and CFA, microbial P cycling in marine sediments has hardly been studied, resulting in a severe lack of information on the genesis and reactivity of sedimentary P_{org}. Consequently, the significance of the benthic microbial P pump to the global P cycle can only be inferred currently using observations of the bulk P pool.

5.2. The impact of animals on P burial

Our results show that sediments on the modern marine shelf that are mixed and ventilated by bioturbation and bioirrigation are around 50 % more efficient at retaining P than sediments under anoxic bottom waters, with net P_{reac} accumulation rates of 35 and 23 μmol m^{-2} d^{-1}, respectively (Fig. 2). The P_{reac} burial flux scales positively with O_2 availability (solid black curve, Fig. 4a; the grey shaded area shows the range of P burial expected for all values of f_{poly}), and the effect of O_2 is stronger for sediments that are more intensively reworked by bioturbation and bioirrigation (dashed black curves). The direct contribution of bioturbation and bioirrigation is shown by observing the lower P_{reac} accumulation rates in simulations without benthic infauna (dashed blue curves in Fig. 3 and Fig. 4a). It is interesting to note that here the burial flux initially decreases for O_2 < 20 μM due to a weak microbial P pump and preferential dissolution of P_{org} by aerobic respiration (Fig. 4a). A reversal in P_{reac} burial when O_2 > 20 μM marks the point where synthesis and burial of $P_{org\text{-}U}$ begins to mitigate

552 the PO_4^{3-} flux to the bottom water. P_{reac} burial in model runs with mixing but without microbial P
553 uptake are even lower (dashed red curves in Fig. 3 and Fig. 4).

554 These results demonstrate that enhanced P burial may not only be driven by O_2 availability, as
555 assumed in some modeling studies (Van Cappellen and Ingall, 1994; Slomp and Van Cappellen,
556 1994), but requires the intervention of P-storing microorganisms and animals to churn and ventilate
557 the sediment. Enhanced P burial in oxic sediments with faunal communities is explained
558 mechanistically as follows. First, bioturbation limits diffusive PO_4^{3-} fluxes to the bottom water by
559 shunting highly labile P_{org} away from the aerobic sediment layers where mineralization rates are
560 elevated. This can be appreciated by noting that P_{org} mineralization rates in the top millimeter of
561 bioturbated sediments are several-fold lower than for non-bioturbated sediments, whereas the opposite
562 is true below this depth (Fig. 5). Sub-surface mineralization of P_{org} helps to trap P within the sediment
563 by sink-switching. Without bioturbation, P_{org} can only be transported downwards by the relatively
564 slow process of burial, allowing more P_{org} to be solubilized to PO_4^{3-} at the sediment-water interface
565 and released back to the ocean. Slomp et al. (1996) similarly proposed that P trapping in North
566 Atlantic slope sediments is favored by the downward mixing of iron-bound P by infauna followed by
567 sink-switching to CFA. Our result is partly dependent on the reverse conveyor belt feeding
568 mechanism of bioturbation (see *2. Model*). It is likely, however, that other bioturbation formalisms
569 result in a similar redistribution of labile P_{org}, although we have not tested these explicitly.

570 Second, seawater pumping into the sediment by bioirrigation enhances nitrification and creates a more
571 favorable niche for P-storing bacteria by deepening the nitrogenous sediment zone relative to
572 oxidized, non-mixed sediments (compare green and dashed blue curve, Fig. 3b). This result is partly
573 dependent on the kinetics of nitrate (NO_X) consumption and the irrigation coefficient, $\alpha(0)$, that are
574 somewhat poorly constrained at the global scale. Deeply-burrowing polychaetes can result in large
575 nitrate penetration depths (Dale et al., 2011; Renz and Forster, 2014), although not all irrigated
576 sediments show the same features (Devol and Christensen, 1993; Dale et al., 2014). In reality, patterns
577 of solute transport in and around burrows are much more complex than portrayed with the simple
578 irrigation model used here. The thickness of the oxic and nitrogenous zones will depend on many
579 physical and biological factors such as the sediment permeability, bottom water currents and the
580 ecology of each animal species. Nonetheless, the deeper nitrogenous zone with versus without
581 animals supports the proposed rate formulation for P_{poly} synthesis (Eq. (12)). Again, it is important to
582 stress that Eq. (12) is purely conceptual, although it does conform to the known redox window over
583 which microbial P sequestration occurs (Davelaar, 1993). It should also be noted that O_2
584 concentrations with animals are also on average 50 % higher than in the case without them (Fig. 3a).
585 Inclusion of O_2 into Eq. (12), for example by making P_{poly} synthesis dependent on the sum of NO_X +
586 O_2, would require recalibration of the rate constant, k_{30}, but would not fundamentally alter the main
587 results.

588

589 *5.3. Implications for P burial in the early Paleozoic*

590 We modified the model to assess the dynamics of P burial in the early Paleozoic to test the hypothesis
591 advanced by Boyle et al. (2014) that colonization of the continental shelves by bioturbating and
592 burrowing animals at some time between the Ediacaran and early Paleozoic resulted in enhanced P
593 burial. A more nuanced view is now emerging in the palaeontological literature, in which the full
594 scale of the "Cambrian substrate revolution" may have been delayed, perhaps until as late as the
595 Ordovician-Silurian boundary or late Silurian (Tarhan et al., 2015). In other words, there may have
596 been a delay between the appearance of the first trace fossils and quantitatively significant mixing of
597 continental shelf sediments (Tarhan and Droser, 2014).

598 Although the timing and trajectory of the spread of faunal invasion of sediments is still being worked
599 out, it seems certain that at some point between ca. 550 Ma and 420 Ma the bioturbation intensity and
600 burrow depth increased. There is high uncertainty in assigning real numbers to these parameters, and
601 the consensus on this issue is evolving. Mángano and Buatois (2014) reported an increase in
602 maximum burrow depth from around 1 to 6 cm across the Ediacaran/ Paleozoic boundary based on
603 trace fossil specimen analysis. In contrast, sedimentological data suggest that burrow depths in the
604 lower Cambrian never exceeded 3 cm, and bed thicknesses point toward millimetre-scale mixing
605 depths in the lower to middle Cambrian (ca. 542 – 507 Ma) increasing to 1 – 2 cm in the Ordovician –
606 Silurian (ca. 450 – 420 Ma) (Tarhan and Droser, 2014). Clearly, sediment mixing and burrowing
607 depths during the early Cambrian were significantly lower than they are on ocean margins today.

608 In accordance with these latest data, the mixed depth was reduced to 0.5 cm (z_{bt} = 0.25 cm).
609 Bioirrigation was also reduced so that the burrow flushing intensity at 2 cm depth was ~10% of the
610 surface value (z_{bio} = 1 cm). P burial is insensitive to lower z_{bio} values since solute transport in the
611 uppermost sediment layer is dominated by diffusive exchange with the bottom water. To account for
612 the lower bioturbation intensity in sediments this time, the sediment mixing intensity ($D_b(0)$) was
613 decreased arbitrarily from 27 to 5 $cm^2\ yr^{-1}$ and bioirrigation ($\alpha(0)$) from 465 y^{-1} to 50 y^{-1}. Due to the
614 near-impossibility of constraining these latter values accurately, the model focuses on a qualitative
615 comparison between sediments with and without indwelling fauna in the early Paleozoic.

616 The paleo simulations also account for the different boundary conditions at the sediment-water
617 interface. Geochemical evidence that is interconnected with ancient ocean redox status allows some
618 essential features to be reasonably well described (Och and Shields-Zhou, 2012). The deep ocean in
619 the early Paleozoic was ferruginous, with euxinic conditions restricted to the biologically productive
620 margins (Canfield et al., 2008; Li et al., 2010; Lyons et al., 2014). The shallow seas, in contrast, may

621 have been similar to productive regions in the contemporary ocean and experienced oxic bottom
622 waters (Kendall et al., 2012; Lyons et al., 2014).

623 Constraints on global oxygen levels are qualitative at best for this period of Earth's history. Late
624 Ediacaran / early Paleozoic O_2 concentrations and may have been several tens of μM (Canfield et al.,
625 2007; Bjerrum and Canfield, 2011), with anoxic episodes persisting well into the early Paleozoic
626 (Saltzman et al., 2015). As a reflection of this uncertainty, we assessed P burial over the same range
627 of bottom water O_2 concentrations as previously (0 to 150 μM).

628 Sulfate (SO_4^{2-}) concentrations in the early Paleozoic ocean were also much lower than today.
629 Concentrations following the Great Oxygenation Event (2.4 Ga) may have remained at only 1 – 3 mM
630 until the Cambrian or even later, when bioturbation itself may have contributed to a rise in SO_4^{2-} via
631 increased oxidation of sedimentary sulfide (Canfield and Farquhar, 2009; Li et al., 2010; Tarhan et al.,
632 2015). We used a sulfate concentration of 3 mM, and kept all other model parameters at their modern
633 values, including the sedimentation rate. This assumption relates to fact that continental weathering
634 rates at the end of the Ediacaran appear to have been similar to those of today (Maloof et al., 2010;
635 Peters and Gaines, 2012). Sensitivity analysis (not shown) indicates that P burial scales proportionally
636 with sedimentation rate.

637 Knowledge of the flux and lability of organic matter deposited on the sea floor in the early Paleozoic
638 is completely lacking, and we prescribe the contemporary values in the absence of better information.
639 Given that photosynthetic eukaryotes evolved more than 1500 Ma, the biochemical composition and
640 cell size of photosynthesizing biota may have been comparable to today, even though species
641 diversity was lower (Falkowski et al., 2004; Butterfield, 2007; Och and Shields-Zhou, 2012). In that
642 case, particle fluxes would be still be eukaryote-dominated, enhanced by aggregation and ballasting
643 resembling the modern ocean (Lenton et al., 2014). Running the model using the same organic matter
644 flux and reactivity as for the modern scenario will elucidate the impact of ocean chemistry and
645 sediment mixing on P burial. These assumptions can be relaxed if more data becomes available.

646 Model results of the early Paleozoic scenario with bottom water O_2 concentrations of 25 μM show
647 that, in general, the redox structure is not dramatically different from the modern scenario (Fig. S1
648 and S2). Notably, though, the aerobic and nitrogenous layers are less well developed due to the lower
649 bottom water O_2 concentrations, sediment mixing and irrigation rates. Over the range of O_2 levels
650 tested, this causes a decrease in P burial relative to the modern setting mainly as result of lower
651 microbial P_{org} accumulation (black curve in Fig. 4b and Supplement). The results nonetheless show
652 that, even with a much thinner and weakly mixed surface layer, the onset of bioturbation at the low O_2
653 concentrations of some 10s μM believed to characterize this time period (Canfield et al., 2007;
654 Bjerrum and Canfield, 2011) would have increased P burial, shown schematically by the blue arrow in

Fig. 4b. Further increases in the depth of the mixed layer in the late Cambrian lead to even greater burial of P (black arrow).

These results are of qualitative value only due to the assumptions involved in constraining the boundary conditions in ancient sediments. We also assumed for simplicity that the physical aspects of bioturbation, such as particle disaggregation and modification of the sediment fabric as well as feeding mode (local versus non-local), resemble modern sediments. We tested the effect of changes in sediment water content arising from colonization by indwelling fauna. Deckere et al. (2001) observed a lower water content of defaunated versus faunated sediment experiments, and other natural observations have shown that seasonal anoxia and lack of bioirrigation reduces sediment porosity by around 10% (Dale et al., 2013). Anoxic baseline simulations with a 10% lower porosity show a modest decrease in P_{reac} burial from 23 to 18 μmol m^{-2} d^{-1}, driven by an increase in solid fraction mineralization close to the sediment water interface and subsequent loss of PO_4^{3-}. Early sediment colonization may thus have had a greater effect on P_{reac} burial than the baseline model currently predicts.

The oceanic P residence time (ca. 20 kyr, Wallmann, 2010) is relatively short compared to the $>10^5$ years needed for the stabilizing feedbacks on the oceanic P inventory via redox-dependent P burial (Van Cappellen and Ingall, 1994; Lenton and Watson., 2000). Thus, the radiation of indwelling sediment fauna would have helped to lower the oceanic bioavailable P pool over these long time scales, leading to a negative and stabilizing feedback on atmospheric O_2 levels via primary production (Boyle et al., 2014). This could have contributed to a wider stability in the Earth system that may have been necessary for the proliferation of recently developed animal forms that characterize the early Cambrian (Butterfield, 2007; 2009). The results presented here show mechanistically how animals may have 'engineered' the physical, geochemical and microbiological structure of their habitats, leading to stabilizing negative feedbacks with the O_2 levels upon which they depend, with wider implications for the coevolution of the earth system and animal forms (Mermillod-Blondin and Rosenberg, 2006; Butterfield, 2007; 2009; Boyle et al., 2014). In combination with microbial catalysis of bioavailable P into organic compounds, animals very likely exert an important control on the cycling of burial of P in the modern and ancient ocean.

5. Conclusions

Observed C and P burial and recycling rates from the literature interpreted with a diagenetic model strongly suggest that uptake and recycling of P by microorganisms enhances P burial in bioturbated and bioirrigated marine sediments alongside iron-associated phosphorus and authigenic apatite formation. Whilst microbial cycling of P has been recognized for many years by limnologists, and inferred from C_{org}:P_{org} burial ratios and benthic fluxes by marine geochemists, redox-dependent storage and burial of refractory microbial P (termed the microbial P pump) has thus far not been

included in diagenetic models of P cycling in marine sediments. Microbial P sequestration in conjunction with bioturbation intensity and bottom water O_2 levels (summarized in Fig. 4) should be considered when parameterizing redox-dependent benthic P release in global biogeochemical models. O_2 concentration by itself may be insufficient to explain benthic phosphate fluxes in periods in Earth's history when bioturbating and burrowing fauna colonized or recolonized the seafloor. Our results support the notion that the presence of P_{org} in ancient marine sediments could, in part, be due to the synthesis of refractive microbial compounds in surface sediments.

More accurate information regarding the controls on microbial sequestration of porewater PO_4^{3-} by, for example, organic carbon content and reactivity, sedimentation rate and bottom water redox conditions and well as physiological controls on P uptake in natural sediments awaits further study. New approaches to quantify microbial P biomarkers or polyphosphates such as X-ray spectroscopy (XANES) will be invaluable to expand the database on the microbial P content of surface sediments in settings displaying a range of bottom water redox conditions (e.g. Kraal et al., 2015).

Acknowledgements

The authors thank Lidya Tarhan and an anonymous referee for comprehensive and thoughtful reviews and Tim Lyons for the editorial handling. This work is a contribution of the Sonderforschungsbereich 754 "Climate – Biogeochemistry Interactions in the Tropical Ocean" (www.sfb754.de) which is supported by the Deutsche Forschungsgemeinschaft.

References

Algeo, T. J. and Ingall, E. (2007) Sedimentary Corg:P ratios, paleocean ventilation, and Phanerozoic atmospheric pO2. *Palaeogeogr. Palaeoclimatol. Palaeoecol.* **256** , 130-155.

Aller, R. C. and Aller, J. Y. (1992) Meiofauna and solute transport in marine muds. *Limnol. Oceanogr.* **37**, 1018-1033.

Anderson, L. D., Delaney, M. L. and Faul, K. L. (2001) Carbon to phosphorus ratios in sediments: Implications for nutrient cycling. *Glob. Biogeochem. Cy.* **15**, 64-79.

Anschutz, P., Zhong, S. and Sundby, B. (1998) Burial efficiency of phosphorus and the geochemistry of iron in continental margin sediments. *Limnol. Oceanogr.* **43** , 53-64.

Archer, D. E., Morford, J. L. and Emerson, S. R. (2002) A model of suboxic sedimentary diagenesis suitable for automatic tuning and gridded global domains. *Glob. Biogeochem. Cy.* **16**, 1017, doi:10.1029/2000GB001288.

Bale, A. J. Morris, A. W. (1981) Laboratory simulation of chemical processes induced by estuarine mixing: The behaviour of iron and phosphate in estuaries. *Estuar. Coast. Shelf Sci.***13**, 1-10.

Benitez-Nelson, C. R. (2000) The biogeochemical cycling of phosphorus in marine systems. *Earth-Sci. Rev.* **51**, 109-135.

Berner, R. A. (1980) Early Diagenesis: A Theoretical Approach. Princeton University Press, Princeton, 241 pp.

Berner, R. A. and Rao, J. L. (1994) Phosphorus in sediments of the Amazon River and estuary: Implications for the global flux of phosphorus to the sea. *Geochim. Cosmochim. Acta* **58**, 2333-2339.

729 Berner, R. A., Ruttenberg, K. C., Ingall, E. D. and Rao, J. L. (1993) The nature of phosphorus burial in modern
730 marine sediments. In *Interactions of C, N, P and S Biogeochemical Cycles and Global Change*, NATO ASI
731 Ser., Ser. I, vol. 4, (eds. R. Wollast, F. T. Mackenzie, and L. Chou), Springer, Berlin, pp. 365– 378.
732 Bertics, V. J., Sohm, J. A., Treude, T., Chow, C. E. T., Capone, D. G. Fuhrman, J. A., and Ziebis, W. (2010)
733 Burrowing deeper into benthic nitrogen cycling: The impact of bioturbation on nitrogen fixation coupled to
734 sulfate reduction, *Mar. Ecol. Prog. Ser*., **409**, 1–15.
735 Bjerrum, C. J. and Canfield, D. E. (2011) Towards a quantitative understanding of the late Neoproterozoic
736 carbon cycle. *Proc. Natl. Acad. Sci. U.S.A.* **108**, 5542-5547.
737 Borggaard, O. K. (1991) Effects of phosphate on iron oxide dissolution in ethylenediamine-N,N,N'N'-tetraacetic
738 acid and oxalate. *Clays Clay Miner.* **39**, 324-328.
739 Boudreau, B. P. (1986) Mathematics of tracer mixing in sediments; I. Nonlocal mixing and biological conveyor-
740 belt phenomena. *Am. J. Sci.* 286, 161-198.
741 Boudreau, B. P. (1997) *Diagenetic Models and Their Implementation: Modelling Transport and Reactions in*
742 *Aquatic Sediments*, Springer-Verlag, Berlin, 414 pp.
743 Boudreau, B. P., Arnosti, C., Jorgensen, B. B. and Canfield, D. E. (2008) Comment on "Physical Model for the
744 Decay and Preservation of Marine Organic Carbon". *Science* **319**, 1616-1617.
745 Boudreau, B. P. and Ruddick, B. R. (1991) On a reactive continuum representation of organic matter diagenesis.
746 *Am. J. Sci.* **291**, 507-538.
747 Boyle, R. A., Dahl, T. W., Dale, A. W., Shields-Zhou, G. A., Zhu, M., Brasier, M. D., Canfield, D. E. and
748 Lenton, T. M. (2014) Stabilization of the coupled oxygen and phosphorus cycles by the evolution of
749 bioturbation. *Nat. Geosci.* **7**, 671-676.
750 Brock, J. and Schulz-Vogt, H. N. (2010) Sulfide induces phosphate release from polyphosphate in cultures of a
751 marine Beggiatoa strain. *ISME J*. **5**, 497-506.
752 Burdige, D. J. (2006) Geochemistry of Marine Sediments, Princeton Univ. Press, Princeton, N. J.
753 Burdige, D. J. (2007) Preservation of organic matter in marine sediments: controls, mechanisms, and an
754 imbalance in sediment organic carbon budgets? *Chem. Rev.* **107**, 467-485.
755 Butterfield, N. J. (2009) Oxygen, animals and oceanic ventilation: an alternative view. *Geobiology* **7**, 1-7.
756 Canfield, D. E. and Farquhar, J. (2009) Animal evolution, bioturbation, and the sulfate concentration of the
757 oceans. *Proc. Natl. Acad. Sci. U.S.A.* **106**, 8123-8127.
758 Canfield, D. E., Poulton, S. W., Knoll, A. H., Narbonne, G. M., Ross, G., Goldberg, T. and Strauss, H. (2008)
759 Ferruginous conditions dominated later Neoproterozoic deep-water chemistry. *Science* **321**, 949-952.
760 Canfield, D. E., Poulton, S. W. and Narbonne, G. M. (2007) Late-Neoproterozoic deep-ocean oxygenation and
761 the rise of animal life. *Science* **315**, 92-95.
762 Canfield, D. E., Raiswell, R. and Bottrell, S. (1992) The reactivity of sedimentary iron minerals toward sulfide.
763 *Am. J. Sci.* **292**, 659-683.
764 Clark, L. L., Ingall, E. D. and Benner, R. (1998) Marine phosphorus is selectively remineralized. *Nature* **393**,
765 426.
766 Colman, A. S. And Holland, H. D. (2000) The global diagenetic flux of phosphorus from marine sediments to
767 the oceans: redox sensitivity and the control of atmospheric oxygen levels. In Marine Authigenesis: From
768 Global to Microbial, SEPM Special Publication No. 66. 53-75.
769 Colman, A. S., Mackenzie, F. T. and Holland, H. D. (1997) Redox stabilization of the atmosphere and oceans
770 and marine productivity. *Science* **275**, 406-408.
771 Dale, A. W., Sommer, S., Bohlen, L., Treude, T., Bertics, V. J., Bange, H. W., Pfannkuche, O., Schorp, T.,
772 Mattsdotter, M. and Wallmann, K. (2011) Rates and regulation of nitrogen cycling in seasonally hypoxic
773 sediments during winter (Boknis Eck, SW Baltic Sea): sensitivity to environmental variables. *Est. Coast.*
774 *Shelf Sci.* 95, 14-28.
775 Dale, A. W., Bertics, V. J., Treude, T., Sommer, S. and Wallmann, K. (2013) Modeling benthic–pelagic nutrient
776 exchange processes and porewater distributions in a seasonally hypoxic sediment: evidence for massive
777 phosphate release by *Beggiatoa*? *Biogeosciences* **10**, 629-651, doi:10.5194/bg-10-629-2013.
778 Dale, A. W., Nickelsen L., Scholz, F., Hensen, C., Oschlies, A. and Wallmann, K. (2015a) A revised global
779 estimate of dissolved iron fluxes from marine sediments. *Glob. Biogeochem. Cy.* **29**, doi:
780 10.1002/2014GB005017.
781 Dale, A. W., Sommer, S., Lomnitz, U., Montes, I., Treude, T., Liebetrau, V., Gier, J. , Hensen, C., Dengler, M.,
782 Stolpovsky, K., Bryant, L. D. and Wallmann, K. (2015b) Organic carbon production, mineralisation and
783 preservation on the Peruvian margin. *Biogeosciences* **12**, 1537-1559.
784 Davelaar, D. (1993) Ecological significance of bacterial polyphosphate metabolism in sediments. *Hydrobiologia*
785 **253**, 179-192.
786 De Deckere, E., Tolhurst, T. J. and de Brouwer, J. F. C. (2001) Destabilization of cohesive intertidal sediments
787 by infauna. *Estuar. Coast. Shelf Sci*. **53**, 665-669.

Delaney, M. L. (1998) Phosphorus accumulation in marine sediments and the oceanic phosphorus cycle. *Glob. Biogeochem. Cy.* **12**, 563–572, doi:10.1029/98GB02263.

Demaison, G. J. and Moore, G. T. (1980) Anoxic environments and oil source bed genesis. *Am. Assoc. Pet. Geol. Bull.* **64**, 1179-1209.

Devol, A. H. And Christensen, J. P. (1993) Benthic fluxes and nitrogen cycling in sediments of the continental margin of the eastern North Pacific. *J. Mar. Res.* 51, 345-372.

Diaz, J., Ingall, E., Benitez-Nelson, C., Paterson, D., de Jonge, M. D., McNulty, I. and Brandes, J. A. (2008) Marine polyphosphate: a key player in geologic phosphorus sequestration. *Science* **320**, 652-655.

Diaz, J. M. and Ingall, E. D. (2010) Fluorometric quantification of natural inorganic polyphosphate. *Environ. Sci. Technol.* **44**, 4665-4671.

Diaz, J. M., Ingall, E. D., Snow, S. D., Benitez-Nelson, C. R., Taillefert, M. and Brandes, J. A. (2012) Potential role of inorganic polyphosphate in the cycling of phosphorus within the hypoxic water column of Effingham Inlet, British Columbia. *Glob. Biogeochem. Cy.* **26**, GB2040, doi:10.1029/2011GB004226.

Falkowski, P. G., Katz, M. E., Knoll. A. K., Quigg, A., Raven, J. A., Schofield, O. and Taylor, F. J. R. (2004) The evolution of modern eukaryotic phytoplankton. *Science* **305**, 354-360.

Faul, K. L., Paytan, A. and Delaney, M. L. (2005) Phosphorus distribution in sinking oceanic particulate matter. *Mar. Chem.* **97**, 307-333.

Filippelli, G. M. (2001) Carbon and phosphorus cycling in anoxic sediments of the Saanich Inlet, British Columbia. *Mar. Geol.* **174**, 307-321.

Filippelli, G. M. and Delaney, M. L. (1996) Phosphorus geochemistry of equatorial Pacific sediments. *Geochim. Cosmochim. Acta* **60**, 1479-1495.

Fossing, H., Ferdelman, T. G., and Berg, P. (2000) Sulfate reduction and methane oxidation in continental margin sediments influenced by irrigation (South-East Atlantic off Namibia). *Geochim. Cosmochim. Acta* **64**, 897-910.

Froelich, P., Arthur, M. A., Burnett, W. C., Deakin, M., Hensley, V., Jahnke, R., Kaul, N., Kim, K. H., Roe, K., Soutar, A. and Vathakanon, C. (1988) Early diagenesis of organic matter in Peru continental margin sediments: Phosphorite precipitation. *Mar. Geol.* **80**, 309-343.

Froelich, P. N., Bender, M. L., Luedtke, N. A., Heath, G. R. and DeVries, T. (1982) The marine phosphorus cycle. *Am. J. Sci.* **282**, 474-511.

Froelich, P. N., Kim, K. H., Jahnke, R., Burnett, W. C., Soutar, A. and Deakin, M. (1983) Pore water fluoride in Peru continental margin sediments: Uptake from seawater. *Geochim. Cosmochim. Acta* **47**, 1605-1612.

Froelich, P. N., Klinkhammer, G. P., Bender, M. L., Luedtke, N. A., Heath, G. R., Cullen, D. and Dauphin, P. (1979) Early oxidation of organic matter in pelagic sediments of the eastern equatorial Atlantic: suboxic diagenesis. *Geochim. Cosmochim. Acta* **43**, 1075-1090.

Gachter, R. and Meyer, J. S. (1993) The role of microorganisms in mobilization and fixation of phosphorus in sediments. *Hydrobiologia* **253**, 103-121.

Gachter, R., Meyer, J. S. and Mares, A. (1988) Contribution of bacteria to release and fixation of phosphorus in lake sediments. *Limnol. Oceanogr.* **33**, 1542-1558.

Glud, R. N. (2008) Oxygen dynamics of marine sediments. *Mar. Biol. Res.* **4**, 243-289.

Hartnett H. E., Keil R. G., Hedges J. I. and Devol A. H. (1998) Influence of oxygen exposure time on organic carbon preservation in continental margin sediments. *Nature* **391**, 572-574.

Hedges, J. I., Hu, F. S., Devol, A. H., Hartnett H. E., Tsamakis, E. and Keil, R. G. (1999) Sedimentary organic matter preservation: A test for selective degradation under oxic conditions. *Am. J. Sci.* **299**, 529-555.

Houben, G. J. (2003) Iron oxide incrustations in wells. Part 1: genesis, mineralogy and geochemistry. *App. Geochem.* **18**, 927-939.

Hupfer, M., Rube, B. and Schmieder, P. (2004) Origin and diagenesis of polyphosphate in lake sediments: A P-31-NMR study. *Limnol. Oceanogr.* **49**, 1-10.

Ingall, E. and Jahnke, R. (1994) Evidence for enhanced phosphorus regeneration from marine sediments overlain by oxygen depleted waters. *Geochim. Cosmochim. Acta* **58**, 2571-2575. 1994.

Ingall, E. and Jahnke, R. (1997) Influence of water-column anoxia on the elemental fractionation of carbon and phosphorus during sediment diagenesis. *Mar. Geol.* **139**, 219-229.

Ingall, E., Kolowith, L., Lyons, T. and Hurtgen, M. (2005) Sediment carbon, nitrogen and phosphorus cycling in an anoxic fjord, Effingham Inlet, British Columbia. *Am. J. Sci.* **305**, 240-258.

Ingall, E. D., Bustin, R. M. and Van Cappellen, P. (1993) Influence of water column anoxia on the burial and preservation of carbon and phosphorus in marine shales. *Geochim. Cosmochim. Acta* **57**, 303-316.

Ingall, E. D. and Van Cappellen, P. (1990) Relation between sedimentation rate and burial of organic phosphorus and organic carbon in marine sediments. *Geochim. Cosmochim. Acta* **54**, 373-386.

Jahnke, R. A., Emerson, S. R., Roe, K. K., and Burnett, W. C. (1983) The present day formation of apatite in Mexican continental margin sediments. *Geochim. Cosmochim. Acta* **47**, 259-266.

Jennings, S., Melin, F., Blanchard, J. L., Forster, R. M., Dulvy, N. K. and Wilson, R. W. (2008) Global-scale predictions of community and ecosystem properties from simple ecological theory. *Proc. R. Soc. B.* **275**, 1375-1383.

Jensen, H. S., Mortensen P. B., Andersen F. O. and Rasmussen E. (1995) Phosphorus cycling in a coastal marine sediment, Aarhus Bay, Denmark. *Limnol. Oceanogr.* **40**, 908-917.

Jensen, H. S. and Thamdrup, B. (1993) Iron-bound phosphorus in marine sediments as measured by bicarbonate-dithionite extraction. Hydrobiologia **253**, 47-59.

Jilbert, T., Slomp, C. P., Gustafsson, B. G. and Boer, W. (2011) Beyond the Fe-P-redox connection: preferential regeneration of phosphorus from organic matter as a key control on Baltic Sea nutrient cycles. *Biogeosciences* **8**, 1699-1720.

Johnston, D. T., Poulton, S. W., Goldberg, T., Sergeev, V. A., Podkovyrov, V., Vorob'eva, N. G. , Bekker, A. and Knoll, A. H. (2012) Late Ediacaran redox stability and metazoan evolution. *Earth Planet. Sci. Lett.* **335-336**, 25-35. 2012.

Jordan, T. E., Cornwell, J. C., Boynton, W. R. and Anderson, J. T. (2008) Changes in phosphorus biogeochemistry along an estuarine salinity gradient: The iron conveyer belt. *Limnol. Oceanogr.* **53**, 172-184.

Kendall, B., Anbar, A. D., Kappler, A. and Konhauser, K. O. (2012) The global iron cycle. In *Fundamentals of Geobiology* (eds A. H. Knoll, D. E. Canfield and K. O. Konhauser), John Wiley and Sons, Ltd, Chichester, UK. doi: 10.1002/9781118280874.ch6.

Kraal, P., Slomp, C. P., Reed, D. C., Reichart, G.-J. and Poulton, S. W. (2012) Sedimentary phosphorus and iron cycling in and below the oxygen minimum zone of the northern Arabian Sea. *Biogeosciences* **9**, 2603-2624.

Kraal, P., Bostick, B. C., Reichart, G.-J. and Slomp, C. P. (2015) Characterization of phosphorus species in sediments from the Arabian Sea oxygen minimum zone: Combining sequential extractions and X-ray spectroscopy. *Mar. Chem.* **168**, 1-8.

Krajewski K. P., Van Cappellen P., Trichet J., Kuhn O., Lucas J., Martin-Algarra A., Prévot L., Tewari V. C., Gaspar L., Knight R. I. and Lamboy M. (1994) Biological processes and apatite formation in sedimentary environments. *Eclogae Geol. Helv.* **87**, 701-745.

Krom, M. D. and Berner, R. A. (1981) The diagenesis of phosphorus in a nearshore marine sediment. *Geochim. Cosmochim. Acta* **45**, 207-216.

Kulaev, I. and Kulakovskaya, T. (2000) Polyphosphate and phosphate pump. *Ann. Rev. Microbiol.* **54**, 709-734.

Lebo, M. E. Particle-bound phosphorus along an urbanized coastal plain estuary. *Mar. Chem.* **34**, 225-246. 1991.

Lenton, T. M., Boyle, R. A., Poulton, S. W., Shields-Zhou, G. A. and Butterfield, N. J. (2014) Co-evolution of eukaryotes and ocean oxygenation in the Neoproterozoic era. *Nat. Geosci.* **7**, 257-265.

Lenton, T. M. and Watson, A. J. (2000) Redfield revisited 2. What regulates the oxygen content of the atmosphere? *Glob. Biogeochem. Cy.* **14**, 249-268.

Levin, L. A. and Gage, J. D. (1998) Relationships between oxygen, organic matter and the diversity of bathyal macrofauna. *Deep-Sea Res. Part II* **45**, 129-163.

Li, C., Love, G. D., Lyons, T. W., Fike, D. A., Sessions, A. L. and Chu, X. (2010) A stratified redox model for the Ediacaran ocean. *Science* **328**, 80-83.

Lijklema, L. (1980) Interaction of orthophosphate with iron(III) and aluminum hydroxides. *Env. Sci. Technol.* **14**, 537-541.

Lucotte, M. and D'Anglejan, B. (1983) Forms of phosphorus and phosphorus iron relationships in the suspended matter of the St. Lawrence estuary. *Canad. J. Earth Sci*. **20**, 1880-1890.

Lyons, T. W., Reinhard, C. T., Love, G. D. and Xiao, S. (2012) Geobiology of the Proterozoic Eon. In *Fundamentals of Geobiology* (eds A. H. Knoll, D. E. Canfield and K. O. Konhauser), John Wiley and Sons, Ltd, Chichester, UK. doi: 10.1002/9781118280874.ch20.

Lyons, T. W., Reinhard, C. T. and Planavsky, N. J. (2014) The rise of oxygen in Earth's early ocean and atmosphere. *Nature* **506**, 307-315.

Maloof, A. C., Porter, S. M., Moore, J. L., Dudas, F. O., Bowring, S. A., Higgins, J. A., Fike, D. A. and Eddy, M. P. (2010) The earliest Cambrian record of animals and ocean geochemical change. *Geolog. Soc. Am. Bull.* **122**, 1731-1774.

Meile, C. and Van Cappellen, P. (2005) Particle age distributions and O_2 exposure times: Timescales in bioturbated sediments. *Glob. Biogeochem. Cy.* **19**, GB3013, doi:10.1029/2004GB002371.

Mermillod-Blondin, F. and Rosenberg, R. (2006) Ecosystem engineering: the impact of bioturbation on biogeochemical processes in marine and freshwater benthic habitats. *Aquat. Sci.* **68**, 434-442.

Meysman, F. J. R., Boudreau, B. P., and Middelburg, J. J. (2003) Relations between local, nonlocal, discrete and continuous models of bioturbation. *J. Mar. Res.* **61**, 391-410.

Meysman, F. J. R., Middelburg, J. J. and Heip, C. H. R. (2006) Bioturbation: a fresh look at Darwin's last idea. *Trends Ecol. Evol.* **21**, 688-695.

Middelburg, J. J. (1989) A simple rate model for organic matter decomposition in marine sediments. *Geochim. Cosmochim. Acta* **53**, 1577-1581.
Middelburg, J. J. and Levin, L. A. (2009) Coastal hypoxia and sediment biogeochemistry. *Biogeosciences* 6, 1273-1293.
Mángano, M. G. and Buatois, L. A. (2015) Decoupling of body-plan diversification and ecological structuring during the Ediacaran–Cambrian transition: evolutionary and geobiological feedbacks. *Proc. R. Soc. B*. **281**, 20140038.
Noffke, A., Hensen, C., Sommer, S., Scholz, F., Bohlen, L., Mosch, T., Graco, M. and Wallmann, K. (2012) Benthic iron and phosphorus fluxes across the Peruvian oxygen minimum zone. *Limnol. Oceanogr.* **57**, 851-867.
Och, L. M. and Shields-Zhou, G. A. (2012) The Neoproterozoic oxygenation event: Environmental perturbations and biogeochemical cycling. *Earth-Sci. Rev.* **110**, 26-57.
Papineau, D. (2010) Global biogeochemical changes at both ends of the Proterozoic: insights from phosphorites. *Astrobiology* **10**, 165-181.
Paytan, A., Cade-Menun, B. J., McLaughlin, K. and Faul, K. L. (2003) Selective phosphorus regeneration of sinking marine particles: evidence from ^{31}P-NMR. *Mar. Chem.* **82**, 55-70.
Paytan, A. and McLaughlin, K. (2007) The oceanic phosphorus cycle. Chemical Reviews **107**, 563-576.
Peters, S. E. and Gaines, R. R. (2012) Formation of the 'Great Unconformity' as a trigger for the Cambrian explosion. *Nature* **484**, 363-366.
Poulton, S. W. and Canfield, D. E. (2006) Co-diagenesis of iron and phosphorus in hydrothermal sediments from the southern East Pacific Rise: Implications for the evaluation of paleoseawater phosphate concentrations. *Geochim. Cosmochim. Acta* **70**, 5883-5898.
Poulton, S. W., Krom, M. D. and Raiswell, R. (2004) A revised scheme for the reactivity of iron (oxyhydr)oxide minerals towards dissolved sulfide. *Geochim. Cosmochim. Acta* **68**, 3703-3715.
Reed, D. C., Slomp, C. P. and Gustafsson, B. G. (2011) Sedimentary phosphorus dynamics and the evolution of bottom-water hypoxia: A coupled benthic–pelagic model of a coastal system. *Limnol. Oceanogr.* **56**, 1075-1092.
Renz, J. R. and Forster, S. (2014) Effects of bioirrigation by the three sibling species of *Marenzelleria* spp. on solute fluxes and porewater nutrient profiles. *Mar. Ecol. Prog. Ser*. 505, 145-159.
Robbins, J. A. (1986) A model for particle-selective transport of tracers in sediments with conveyor belt deposit feeders. *J. Geophys. Res*. 91, 8542-8558.
Ruttenberg, K. C. (2014) The global phosphorus cycle. In *Treatise on Geochemistry Volume 10*, (eds. H. D. Holland and K. K. Turekian), Elsevier, p 499-558.
Ruttenberg, K. C. and Berner, R. A. (1993) Authigenic apatite formation and burial in sediments from non-upwelling, continental margin environments. *Geochim. Cosmochim. Acta* **57**, 991-1007.
Ruttenberg, K. C. and Goni, M. A. (1997) Phosphorus distribution, C:N:P ratios, and $\delta^{13}C_{OC}$ in arctic, temperate, and tropical coastal sediments: Tools for characterizing bulk sedimentary organic matter. *Mar. Geol.* **139**, 123-145.
Saltzman, M. R., Edwards, E. T., Adrain, J. M. And Westrop, S. R. (2015) Persistent oceanic anoxia and elevated extinction rates separate the Cambrian and Ordovician radiations. *Geology*, 43, 807-810.
Sannigrahi, P. and Ingall, E. (2005) Polyphosphates as a source of enhanced P fluxes in marine sediments overlain by anoxic waters: Evidence from ^{31}P NMR. *Geochem. Trans.* **6**, 52.
Sarmiento, J. L. and Gruber, N. (2006) Ocean Biogeochemical Dynamics. Princeton University Press, Princeton, 526 pp.
Schenau, S. J. and de Lange, G. J. (2001) Phosphorus regeneration vs. burial in sediments of the Arabian Sea. *Mar. Chem.* **75**, 201-217.
Schenau, S. J., Reichart, G. J. and de Lange, G. J. (2005) Phosphorus burial as a function of paleoproductivity and redox conditions in Arabian Sea sediments. *Geochim. Cosmochim. Acta* **69**, 919-931.
Schuffert, J. D., Jahnke, R. A., Kastner, M., Leather, J., Sturz, A. and Wing, M. R. (1994) Rates of formation of modern phosphorite off western Mexico. *Geochim. Cosmochim. Acta* **58**, 5001-5010.
Schulz, H. N. and Schulz, H. D. (2005) Large sulfur bacteria and the formation of phosphorite. *Science* **307**, 416-418.
Shapiro, J. (1967) Induced rapid release and uptake of phosphate by microorganisms. Science **155**, 1269-1271.
Shen, Y. N., Zhang, T. G. and Hoffman, P. F. (2008) On the coevolution of Ediacaran oceans and animals. *Proc. Natl. Acad. Sci. U.S.A.* **105**, 7376-7381.
Slomp, C. P. (2011) Phosphorus cycling in the estuarine and coastal zones: sources, sinks, and transformations. In *Treatise on Estuarine and Coastal Science 5* (eds. E. Wolanksi and D. McLusky), 201-229.
Slomp, C. P., Epping, E. H. G., Helder, W. and Van Raaphorst, W. (1996) A key role for iron-bound phosphorus in authigenic apatite formation in North Atlantic continental platform sediments. *J. Mar. Res.* **54**, 1179-1205.

967 Slomp, C. P., Thomson, J. and de Lange, G. J. (2004) Controls on phosphorus regeneration and burial during
968 formation of eastern Mediterranean sapropels. *Mar. Geol.* **203**, 141-159.
969 Slomp, C. P. and Van Cappellen, P. (2007) The global marine phosphorus cycle: sensitivity to oceanic
970 circulation. *Biogeosciences* **4**, 155-171.
971 Smith, J. N., Boudreau, B. P. And Noshkin, V. (1986) Plutonium and ^{210}Pb distributions in northeast Atlantic
972 sediments: subsurface anomalies caused by nonlocal mixing. *Earth Planet. Sci. Lett*., **81**, 15-28.
973 Spiteri, C., Van Cappellen, P. and Regnier, P. (2008) Surface complexation effects on phosphate adsorption to
974 ferric iron oxyhydroxides along pH and salinity gradients in estuaries and coastal aquifers. *Geochim.*
975 *Cosmochim. Acta* **72**, 3431-3445.
976 Steenbergh, A. K., Bodelier, P. L. E., Heldal, M., Slomp, C. P., Laanbroek, H. J. (2012) Does microbial
977 stoichiometry modulate eutrophication of aquatic ecosystems? *Env. Microbiol.* 15, 1572-1579.
978 Suess, E. (1981) Phosphate regeneration from sediments of the Peru continental margin by dissolution of fish
979 debris. *Geochim. Cosmochim. Acta* **45**, 577-588.
980 Sun, M. Y., Aller, R. C., Lee, C., & Wakeham, S. G. (2002) Effects of oxygen and redox oscillation on
981 degradation of cell-associated lipids in surficial marine sediments. *Geochim. Cosmochim. Acta* **66**, 2003-
982 2012.
983 Sundby, B., Gobeil, C., Silverberg, N. and Mucci, A. (1992) The phosphorus cycle in coastal marine sediments.
984 *Limnol. Oceanogr.* **37**, 1129-1145.
985 Tarhan, L. G. and Droser, M. L. (2014) Widespread delayed mixing in early to middle Cambrian marine shelfal
986 settings. *Palaeogeogr. Palaeoclimatol. Palaeoecol.* **399**, 310-322.
987 Tarhan, L. G., Droser, M. L., Planavsky, N. J. and Johnston, D. T. (2015) Protracted development of
988 bioturbation through the early Palaeozoic Era. *Nat. Geosci.* **8**, 865-869.
989 Thamdrup, B., Dalsgaard, T., and Revsbech, N. P. (2012) Widespread functional anoxia in the oxygen minimum
990 zone of the Eastern South Pacific. *Deep Sea Research Part I: Oceanographic Research Papers* 65, 36-45.
991 Van Cappellen, P. and Berner, R. A. (1988) A mathematical model for the early diagenesis of phosphorus and
992 fluorine in marine sediments; apatite precipitation. *Am. J. Sci.* **288**, 289-333.
993 Van Cappellen, P. and Ingall, E. D. (1994) Benthic phosphorus regeneration, net primary production, and ocean
994 anoxia: A model of the coupled marine biogeochemical cycles of carbon and phosphorus. *Paleoceanography*
995 **9**, 677-692.
996 Van Cappellen P. and Ingall, E. D. (1997) Redox stabilization of the atmosphere and oceans and marine
997 productivity - Response. *Science* **275**, 407-408.
998 Van Cappellen, P. and Ingall, E. D. (1996) Redox stabilization of the atmosphere and oceans by phosphorus-
999 limited marine productivity. *Science* **271**.
1000 van der Zee, C., Roberts, D. R., Rancourt, D. G. and Slomp, C. P. (2003) Nanogoethite is the dominant reactive
1001 oxyhydroxide phase in lake and marine sediments. *Geology* **31**, 993-996.
1002 Wallmann, K. (2014) Is late Quaternary climate change governed by self-sustained oscillations in atmospheric
1003 CO2? *Geochim. Cosmochim. Acta* **132**, 413-439.
1004 Wallmann, K. (2010) Phosphorus imbalance in the global ocean? *Glob. Biogeochem. Cy.* **24**, GB4030,
1005 doi:10.1029/2009GB003643.
1006 Westrich, J. T. and Berner, R. A. (1984). The role of sedimentary organic matter in bacterial sulfate reduction:
1007 the G-model tested. *Limnol. Oceanogr.* **29**, 236-249.
1008

Figure captions

Fig. 1. Conceptual P cycle in fine-grained, oxic (bioturbated and bioirrigated) continental margin sediments outside of oxygen minimum zones. White squares and circles denote solids and solutes, respectively. Particulate P is added to the sediment as P_{org} and FeP. PO_4^{3-} released to the porewater from these phases is free to be transported out of the sediment by diffusion and bioirrigation. PO_4^{3-} can also be re-precipitated into authigenic FeP and CFA. The extended model considers P cycling by microorganisms (blue arrows). Dissolved PO_4^{3-} can be assimilated into an intracellular polyphosphate pool (P_{poly}). A fraction (f_{poly}) of P_{poly} is transformed into an unreactive particulate organic P phase (P_{org-U}) with the remainder (1-f_{poly}) shunted back to the bulk P_{org} pool. If P_{poly} is mixed or buried below the aerobic sediment layers it is rapidly hydrolyzed back to PO_4^{3-}. The black bars on the right schematically indicate the spatial separation of organic matter respiration by electron acceptors with depth in the bioturbated layer. See Table S4 for stoichiometries of reactions, R.

Fig. 2. Simulated rates of P turnover in (a) oxic and (b) anoxic sediments in modern shelf sediments (μmol m^{-2} d^{-1}). P_{reac} burial fluxes are calculated at 100 cm. The relative magnitude of the fluxes is indicated schematically by the arrow thicknesses.

Fig. 3. Simulated concentrations in modern shelf sediments. (a) Dissolved oxygen, (b) nitrate + nitrite, (c) phosphate, (d) organic C, (e) organic P (including P_{org-U}), (f) iron-associated P, (g) carbonate fluorapatite, and (h) total reactive P. Green and black curves represent scenarios with oxic and anoxic bottom waters, respectively. Dashed red curves show simulation results for oxic sediments without the microbial P pump and thus the effect of animals only (red star in Fig. 4a). The dashed blue curves examine the effect of microbial P without bioturbation and bioirrigation (blue star in Fig. 4a). Despite preferential mineralization of P_{org} in oxic sediment layers, P_{org} concentrations are highest in the oxic scenario due to synthesis of microbial P_{org}. C_{org} concentrations are, in contrast, lower in oxic sediments. P_{org} is absent below the bioturbation zone in the simulation without microbial P synthesis. All geochemical profiles are shown in the Electronic Annex. Note different depth scales.

Fig. 4. Simulated steady state P_{reac} burial flux for sediments over a range of bottom water O_2 concentrations. (a) Modern sediments. Fluxes using the baseline model parameters (Table 2) are shown as black curves with circles, and the grey shaded area shows P burial for the full range of f_{poly} (0 to 1). Results are also shown for a deeper sediment mixing and burrowing (doubling of parameters z_{bt} and z_{bio}), and for more intense mixing and burrowing (doubling of parameters $D_b(0)$ and $\alpha(0)$). The dashed red curve shows P burial without the microbial P pump, whereas the dashed blue curve shows results where bioturbation and bioirrigation are turned off. The stars correspond to the respective sediment profiles in Fig. 3. The green circle shows the anoxic baseline simulation with a lower

porosity (see text). (b) Early Paleozoic sediments. P burial fluxes using the parameters in Table 2 are shown as the black curve and the dashed blue curve is the result without bioturbation and bioirrigation. The red curve is P burial with a deeper 2 cm sediment mixed depth, tentatively applicable to the late Cambrian / Ordovician shelf (z_{bt} = 1 cm, z_{bio} = 1 cm, $D_b(0)$ = 5 cm^2 yr^{-1}, $\alpha(0)$= 50 y^{-1}). The arrows schematically indicate the expected trajectory of P burial following the radiation of deposit feeders and burrowing fauna with bottom water O_2 concentrations believed to characterize the early Paleozoic (Canfield et al., 2007).

Fig. 5. Organic phosphorus mineralization rate (sum of R_1 to R_7, Table S5) in oxic sediments inhabited by fauna (green curve) and oxic sediments without fauna (dashed blue curves). Bioturbation leads to lower rates at the surface and higher rates towards the base of the bioturbated zone, favoring the sequestration of P into authigenic phases including microbial P. The bottom water O_2 concentration is 150 μM in both cases.

Table 1. Observations of C and P geochemistry in oxic and anoxic margin sediments.

	Oxic	Anoxic
C_{org}:P_{org}	30 – 115 [a]	200 – 700 [b]
C_{org}:P_{reac}	21 [c]	54 – 161 [c]
C_{org} burial efficiency (CBE, %)	25 ± 10 [d]	> 40 [e]
P_{org} burial efficiency (PBE, %)	20 – 40 [f]	< 2 – 11 [g]
$(C:P)_{REG}$ [h]	118 ± 24 [i]	< 70 [j]

[a] From the data corresponding to 'oxic sites' in Fig. 3 of Slomp and Van Cappellen (2007).

[b] From the data corresponding to 'low oxygen and anoxic sites' in Fig. 3 of Slomp and Van Cappellen (2007), as well as data from the anoxic Arabian Sea oxygen minimum zone from Kraal et al. (2012). Values exceeding 1000 observed in the paleo record are rare in modern sediments.

[c] Slomp et al. (2004)

[d] Literature data show that CBE depends non-linearly on the sediment mass accumulation rate (e.g. Burdige, 2007) and, possibly, the availability of dissolved oxygen. A mass accumulation rate of 0.075 g cm^{-2} yr^{-1} can be calculated for a typical upper slope / shelf setting using the formula $\rho \cdot (1\text{-}\varphi) \cdot \omega_{acc}$ where ρ (2.5 g cm^{-3}) is the density of sediment particles, and φ (0.7) and ω_{acc} (0.1 cm yr^{-1}) are the porosity and sedimentation rate of compacted sediments, respectively. For oxygenated bottom waters (> 20 μM O_2), this mass accumulation rate corresponds to a CBE of around 25 % (Dale et al., 2015b).

[e] As footnote [d], for < 20 μM O_2

[f] Data on PBE in oxic, bioturbated sediments are scarce and there is high uncertainty in this value. PBE can be estimated using the CBE and C_{org}:P_{org} burial ratios for which more data is available: $PBE_{OX} = \frac{PBE_{AN} \cdot CBE_{OX} \cdot (C_{org}:P_{org})_{AN}}{CBE_{AN} \cdot (C_{org}:P_{org})_{OX}}$, where subscripts 'OX' and 'AN' denote oxic and anoxic sediments, respectively. Assuming average values for CBE_{AN}, PBE_{AN} and $(C_{org}:P_{org})_{AN}$ of 50 %, 7 % and 400, respectively, and CBE_{OX} and $(C_{org}:P_{org})_{OX}$ burial ratios of 25 % and 50 (respectively), PBE_{OX} is 28 ± 14 %, hence the proposed range of 20 – 40. Notwithstanding the uncertainty arising from the input parameters, PBE in oxic sediments is at least a factor of 2 – 4 that in anoxic sediments. For comparison, Jensen et al. (1995) calculated a PBE of 29 – 35 % in oxic Aarhus Bay sediments, whereas Ingall and Jahnke (1994) reported lower PBE in oxic sediments ranging from 6 to 23 % based on a few observations on the continental slope.

[g] For oxygen deficient bottom waters (< 20 μM O_2) (Schenau et al., 2000; Slomp et al., 2004; Ingall and Jahnke, 1994)

[h] Benthic regeneration ratio = DIC flux / PO_4^{3-} flux at sediment surface determined in situ using benthic chambers. It is important to point out that Colman and Holland (2000) caution that benthic phosphate fluxes, and indeed dissolved inorganic carbon fluxes, may exhibit seasonal variability. For the present study, we note these concerns but lay them to one side, and consider that $(C:P)_{REG}$ ratios are indicative of steady state or seasonally-averaged conditions.

[i] Using the empirical transfer function of Wallmann (2010).

[j] Values for anoxic bottom waters on the Peruvian margin range from 4 to 68 (Noffke et al., 2012). The empirical function of Wallmann (2010) based on in situ flux measurements predicts a value of 11 ± 24 for near-anoxic conditions, although the full range of values for anoxic waters is very similar to the Peruvian margin. Sannigrahi and Ingall (2005) report a value of 39 for an anoxic site in Effingham Inlet.

Table 2. Key model parameters for modern oxic sediments displaying bioturbation and bioirrigation. Values for anoxic and early Paleozoic (Pz) settings that differ from these are also given. Parameter sources are given in Table S3.

Description	Value		
	Oxic	Anoxic	Pz
Sediment accumulation rate, ω_{acc} (cm yr^{-1})	0.1		
Surface sediment porosity, $\varphi(0)$ (–)	0.9		
Bioturbation coefficient at sediment surface, $D_b(0)$ (cm^2 yr^{-1}) [a]	28	0.2	5
Bioturbation halving depth, z_{bt} (cm)	3		0.25
Bioirrigation coefficient at sediment surface, $\alpha(0)$ (yr^{-1}) [a]	465	4	50
Bioirrigation attenuation coefficient, z_{bio} (cm)	2		1
Average lifetime of the reactive C_{org} components, a (yr)	3×10^{-4}		
Shape of gamma distribution for C_{org} mineralization, ν (–)	0.05		
Rate constant for precipitation of apatite, k_{29} (yr^{-1})	1		
Rate constant for polyphosphate synthesis, k_{30} (M^{-1} yr^{-1})	3×10^{7}		
Rate constant for polyphosphate hydrolysis, k_{31} (yr^{-1})	50		
Rate constant for transformation of P_{poly} to P_{org}, k_{32} (yr^{-1})	50		
Rate constant for transformation of P_{poly} to $P_{org\text{-}U}$, k_{33} (yr^{-1})	50		
Fraction of P_{poly} converted to $P_{org\text{-}U}$, f_{poly} (–)	0.25		
Fe:P ratio in allochthonous Fe_{HR}, ε_{all} (mol Fe (mol P)$^{-1}$)	25		
Fe:P ratio in authigenic Fe_{HR}, ε_{aut} (mol Fe (mol P)$^{-1}$)	10		
Fe:P ratio in Fe_{MR} recrystallized from Fe_{HR}, ε_{age} (mol Fe (mol P)$^{-1}$)	40		
Equilibrium PO_4^{3-} concentration for CFA precipitation, C_{eq} (µM)	10		
Atomic P-C ratio in deposited organic matter, r_{PC} (mol P (mol C)$^{-1}$)	1/106		
Acceleration factor for aerobic (relative to anaerobic) C_{org} degradation, *foxC* (–)	2		
Acceleration factor for aerobic P_{org} degradation relative to C_{org}, *foxP* (–)	2		
Acceleration factor for anaerobic P_{org} degradation relative to C_{org}, *fanoxP* (–)	2		
Bottom water concentration of O_2 (µM)	150	0.1	Variable [b]
Bottom water concentration of NO_3^- (µM)	35		
Bottom water concentration of SO_4^{2-} (µM)	28000		3000
Bottom water concentration of Fe^{2+} (µM)	0		
Bottom water concentration of PO_4^{3-} (µM)	0		
Bottom water concentration of H_2S (µM)	0		
Seafloor flux of C_{org} (mmol cm^{-2} yr^{-1})	0.34		
Seafloor flux of P_{org} (mmol cm^{-2} yr^{-1})	$0.34/r_{CP}$		
Seafloor flux of Fe_{HR} (mmol cm^{-2} yr^{-1})	0.011		
Seafloor flux of P associated with Fe_{HR} (mmol cm^{-2} yr^{-1})	$0.011//\varepsilon_{all}$		
Seafloor flux of CFA (mmol cm^{-2} yr^{-1})	0		
Seafloor flux of P_{poly} (mmol cm^{-2} yr^{-1})	0		
Seafloor flux of $P_{org\text{-}U}$ (mmol cm^{-2} yr^{-1})	0		

[a] Bioturbation ($D_b(0)$) and bioirrigation ($\alpha(0)$) are scaled to bottom water O_2 concentration (see Table S1) which causes a reduction in the mixing and burrowing intensities as O_2 falls below ca. 20 µM.

[b] For the Paleozoic simulations, a ranges of O_2 from 0.1 to 150 µM is used (Fig. 4).

Table 3. Modelled C and P geochemistry in modern oxic and anoxic shallow margin sediments from the simulations that include the microbial P loop.

	Oxic	Anoxic
C_{org}/P_{org} burial ratio [a, b]	73	497
C_{org}/P_{reac} burial ratio [a]	44	196
C_{org} burial efficiency (CBE, %) [a]	16	47
P_{org} burial efficiency (PBE, %) [a,b]	24	10
Inorganic carbon-to-phosphorus regeneration ratio, $(C:P)_{REG}$	116	63

[a] At 100 cm
[b] Includes P_{org-U}

1111 Fig. 1

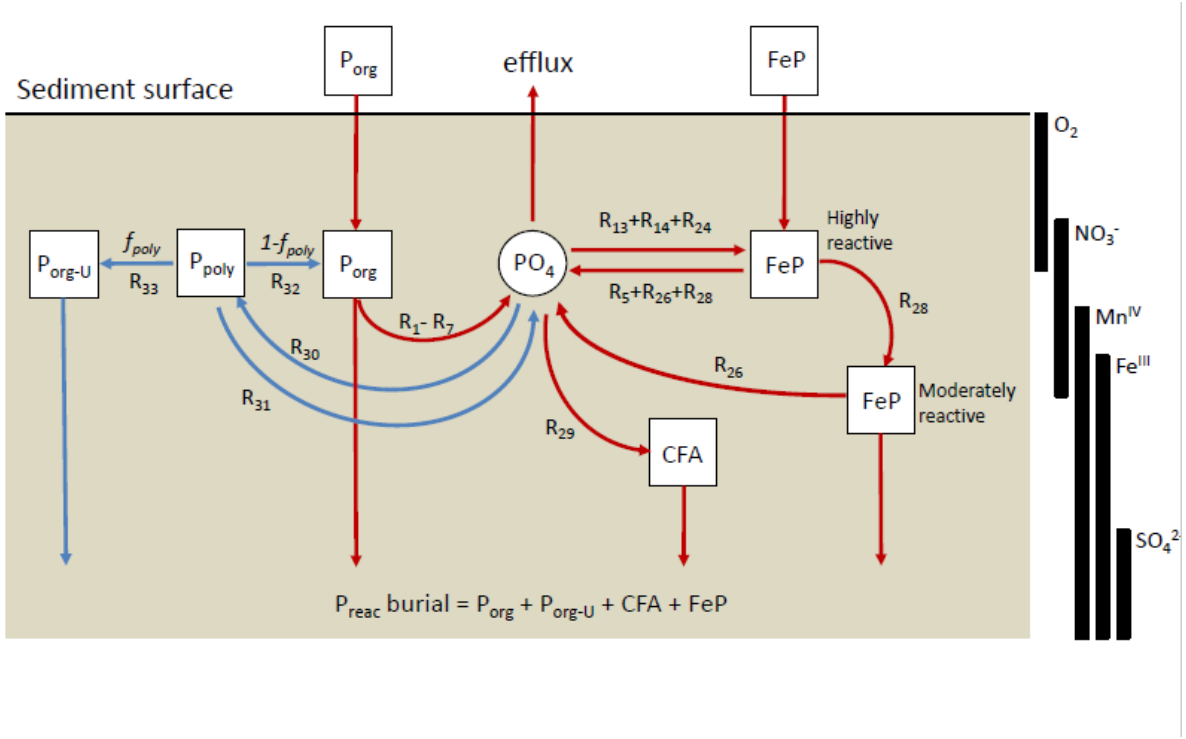

1112

1113

1114 Fig. 2.

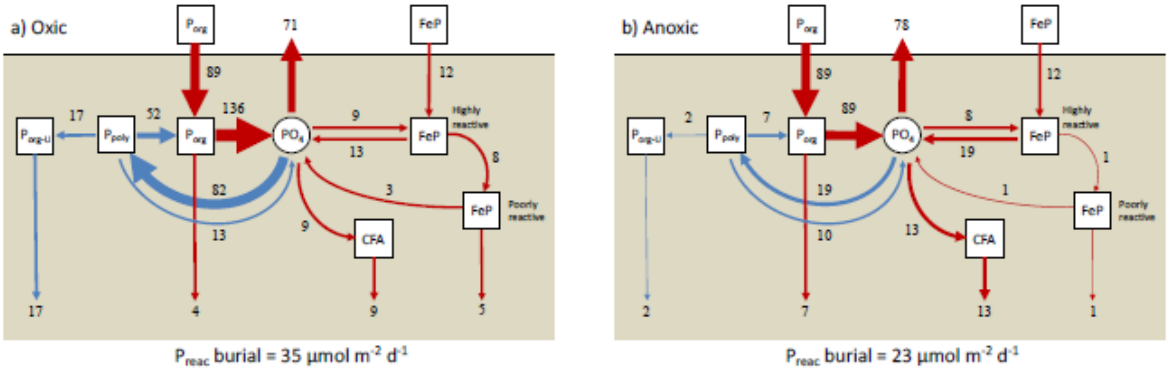

1115

1116

1117 Fig. 3

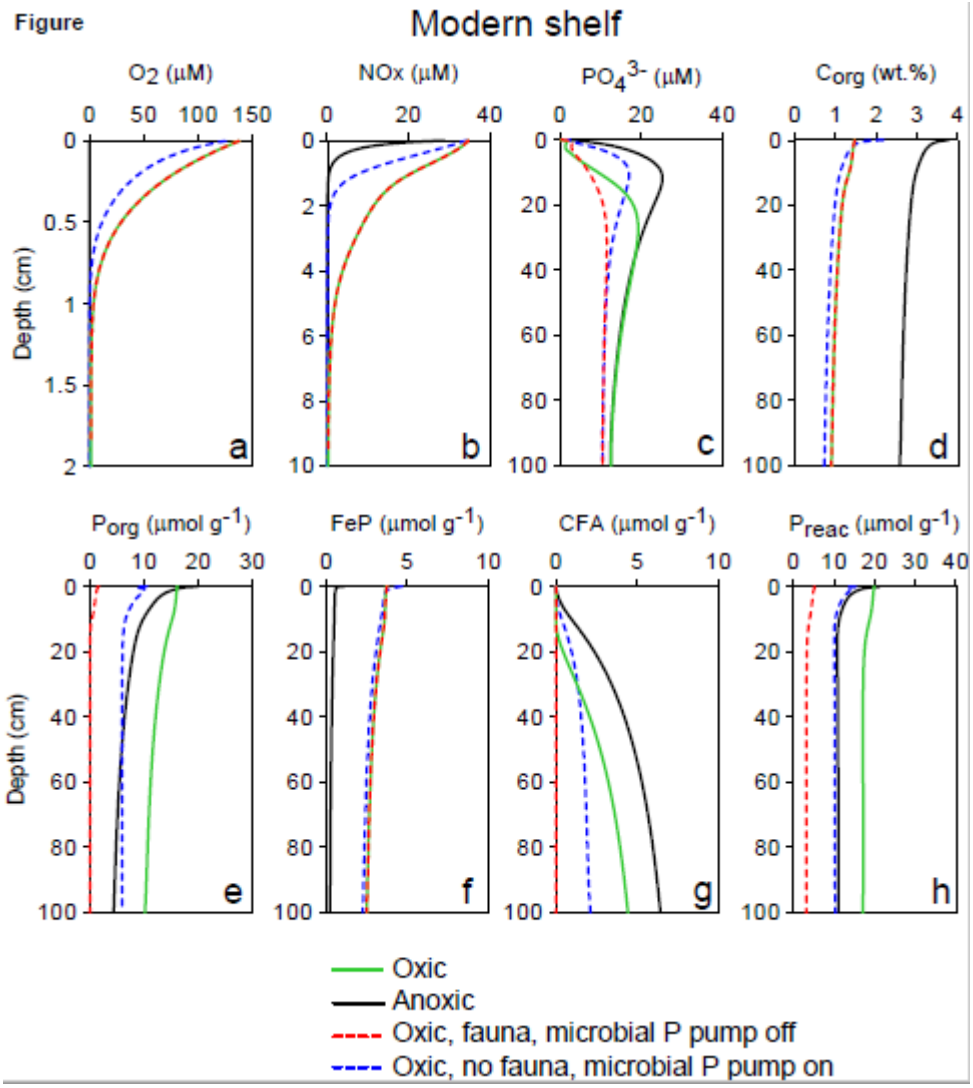

1118

1119

1120 Fig. 4

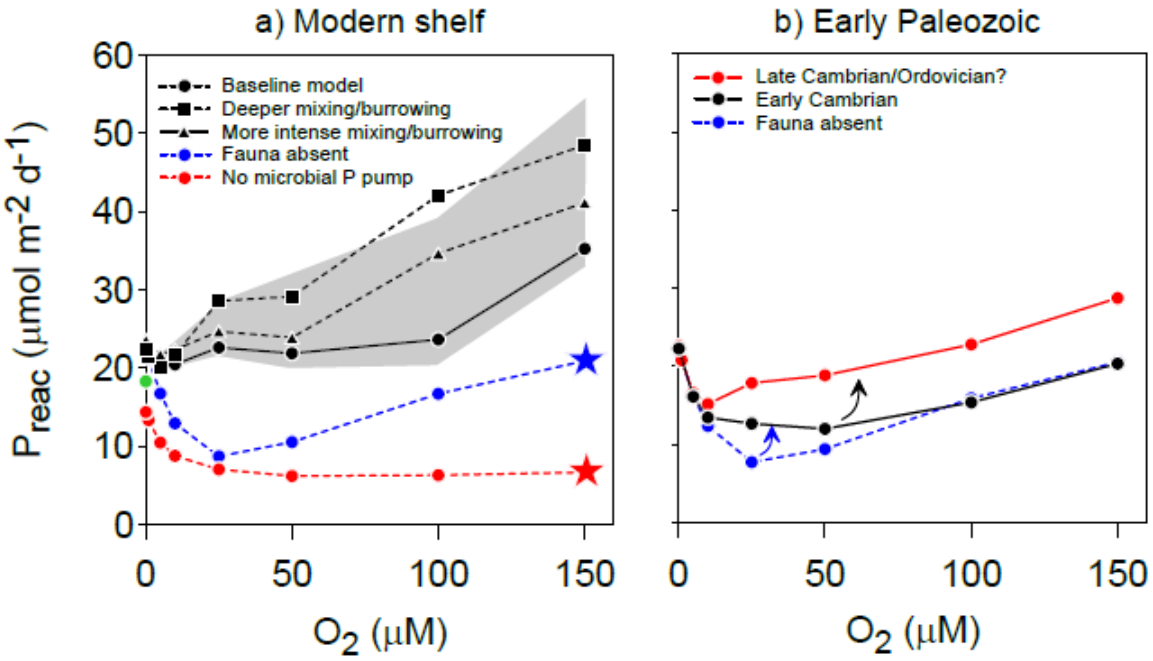

1121

1122

1123 Fig. 5

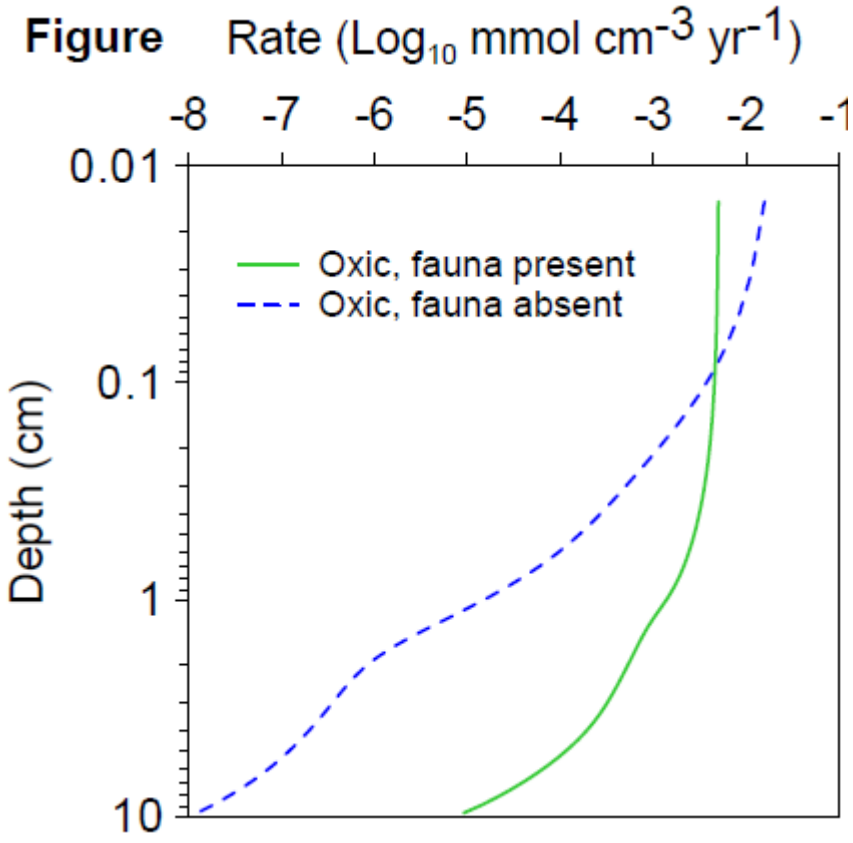

1124